Science of Remote Sensing 12 (2025) 100288

Contents lists available at ScienceDirect

Science of Remote Sensing

journal homepage: www.sciencedirect.com/journal/science-of-remote-sensing

Three-dimensional models of coral microatolls using structure-from-motion photogrammetry and iPhone LiDAR scanning: A fast, reproducible method for collecting relative sea-level data in the field

Nurul Syafiqah Tan [a,b,*], Rohan Gautam [a,b], Fangyi Tan [a,b], Gina M. Sarkawi [a,b], Jędrzej M. Majewski [c], Junki Komori [a,b], Shi Jun Wee [a,d], Khai Ken Leoh [a,b], Lucas D. Koh [a,b], Adam D. Switzer [a,b], Aron J. Meltzner [a,b]

[a] Asian School of the Environment, Nanyang Technological University, Singapore
[b] Earth Observatory of Singapore, Nanyang Technological University, Singapore
[c] Geohazards Research Unit, Institute of Geology, Adam Mickiewicz University, Poznań, Poland
[d] Department of Geographical Sciences, University of Maryland, Maryland, United States

A R T I C L E I N F O

Keywords:
Structure-from-motion photogrammetry
iPhone LiDAR
coral microatoll
3D model
Sea level
Slabbing

A B S T R A C T

Coral microatolls, geological proxies commonly used for reconstructing relative sea-level (RSL) in low-latitude regions, are valued for their precision and ability to continuously track RSL changes through the elevation of successive concentric surface rings. The brief low-tide window prevents rigorous methods for replicating field observations, limiting opportunities for reinterpretation of coral morphology. Additionally, while the extraction of a physical coral slab remains the preferred method for RSL reconstruction, logistical constraints can render it non-viable. When slabbing is possible, the reliability of the reconstructed RSL might be questionable. This study introduces three-dimensional models created using structure-from-motion photogrammetry and iPhone LiDAR scans to facilitate rigorous analysis of coral microatolls. These methods result in accurate and high-resolution documentation of the coral surface, enabling comprehensive and simultaneous analysis of ring structures of multiple microatolls while ensuring results are representative and replicable. Where slabbing is feasible, this method guides the selection of optimal corals that contain the most complete record of RSL change and validates slabbing results. Where slabbing is not viable, this approach provides an alternative means to obtaining RSL histories. Integrating this model-based approach into conventional fieldwork enables extensive data interpretation off-site. Furthermore, the user-friendly nature of these methods enhances accessibility for researchers with limited resources. The benefits and limitations of each technique are also discussed. While photogrammetry-derived point clouds are denser, they necessitate additional georeferencing steps to ensure accurate scale and orientation. Conversely, iPhone-derived models possess inherent scale, though they require additional processing steps, carrying a potential risk of data loss.

1. Introduction

Since the Last Glacial Maximum [e.g. Clark et al., 2009; Mix et al., 2001], there has been an influx of water into the ocean basins from the melting of land-based ice sheets [e.g. Fleming et al., 1998; Peltier, 2002]. However, this distribution is not uniform; amounts and rates differ spatially (Gehrels and Long, 2008; Li et al., 2023; Milne and Mitrovica, 2008; Mitrovica et al., 2011) due to complex processes including glacial isostatic adjustment [e.g. Clark et al., 1978; Lambeck et al., 2014; Peltier, 2004] that can lead to changes in both sea-surface and land height (Camoin and Webster, 2015; Rovere et al., 2016; Whitehouse, 2018). Changes in either sea-surface or land height manifest as changes in relative sea level (RSL), the height of the ocean surface locally relative to a fixed point on land (Gehrels and Long, 2008; Kemp et al., 2015; Khan et al., 2015). Far-field equatorial sites can provide important constraints on changes in global ice volume (Whitehouse, 2018). However, due to glacial and hydro-isostatic adjustment processes (Gehrels and Long, 2008), many tropical coastlines are characterised by

* Corresponding author. Asian School of the Environment, Nanyang Technological University, Singapore.
E-mail address: nurulsya005@e.ntu.edu.sg (N.S. Tan).

https://doi.org/10.1016/j.srs.2025.100288
Received 17 December 2024; Received in revised form 23 July 2025; Accepted 16 September 2025
Available online 17 September 2025

a mid-to late-Holocene RSL fall (Khan et al., 2015; Mitrovica and Milne, 2002), which reduces the accommodation space available for sediment deposition in the region (Kelsey et al., 2015; Li et al., 2023). Coral microatolls offer an alternative means of recording high-resolution continuous RSL histories from far-field regions where the preservation of pristine sedimentary indicators may be limited [e.g. Scoffin and Le Tissier, 1998; Tan et al., 2024].

Coral microatolls are colonies of massive coral that are commonly found in intertidal zones in low-latitude regions (Meltzner and Woodroffe, 2015; Scoffin and Stoddart, 1978) that can serve as proxies for past RSL as their upward growth is limited by low tides (Camoin and Webster, 2015; Goodwin and Harvey, 2008; Woodroffe and McLean, 1990). They form when the uppermost part of a coral colony dies down to a uniform elevation due to prolonged subaerial exposure. However, the parts of the coral below the highest level of survival (HLS) remain alive, growing upward and outward until the coral experiences another diedown. The highest elevation up to which a coral grows in a certain year is termed the highest level of growth (HLG) (Meltzner and Woodroffe, 2015; Meltzner et al., 2017; Wan et al., 2020). The alternating unrestricted upward growth and occasional diedowns result in an upper surface morphology that is characterised by a series of concentric ridges or rings, where the relative elevation of successive rings is indicative of RSL trends as the coral grows (Scoffin and Stoddart, 1978; Majewski et al., 2022; Yu et al., 2009). Unlike most other proxies which offer information about RSL at a single point in time, microatolls continuously track changes in RSL as they grow (Meltzner et al., 2017; Miyata et al., 1990). These characteristics allow microatoll-based reconstructions to fill in temporal gaps in the Holocene record for the region [e.g. Majewski et al., 2022; Tan et al., 2024]. An important complication, however, is that in certain circumstances younger rings grow inward toward the centre of the microatoll and over the surface of older rings, resulting in out-of-sequence interior annuli known as overgrowth (Meltzner and Woodroffe, 2015; Scoffin and Stoddart, 1978). In these instances, critical details of the coral growth history, and therefore of RSL change, are hidden in the interior of the coral, and interpretation of RSL change is not straightforward from the coral surface morphology alone.

One method for reconstructing RSL from a coral microatoll involves the extraction of a vertical cross section through a radius or diameter of the coral through a process referred to as slabbing (Supporting Text S1) [e.g. Meltzner and Woodroffe, 2015; Woodroffe and McLean, 1990; Zachariasen et al., 1999, 2000]. The extracted slab is commonly X-rayed to provide a detailed record of the coral's growth history and diedowns [e.g. Natawidjaja et al., 2004; Philibosian et al., 2014; Weil-Accardo et al., 2016]. This method allows for the reconstruction of RSL with vertical uncertainties on the centimetric scale and at a temporal resolution typically on the order of a decade (Meltzner et al., 2017; Zachariasen et al., 2000). However, several logistical considerations limit the practicality of the slabbing method and have prevented more widespread adoption of this technique. Slabbing might not be feasible at all locations (e.g., in Marine Parks or Conservation Zones) (Majewski, 2017; Meltzner and Woodroffe, 2015; Wan et al., 2020), and, even when viable, it is a slow process, limiting the amount of data that can be collected in a field season. Additionally, practical constraints such as a short low-tide window and manpower shortages can make it challenging to systemically determine whether a coral selected for slabbing will yield the most valuable information. In some cases, it has not been clear whether a slab is representative of coeval corals at the site, calling into question whether those results are replicable. For example, Weil-Accardo et al. (2016) slabbed six living coral microatolls from the Lesser Antilles and found that slabs from the coeval microatolls, even from the same site, do not have identical diedown chronologies. Between 1950 and 1989 AD, some corals recorded more diedowns than other corals. Similar observations were made in living microatolls from Simeulue Island in Indonesia (Meltzner et al., 2010, 2012). Additionally, due to natural variability in growth patterns and responses to environmental changes, corals that undergo the same RSL histories can sometimes exhibit different surface morphologies (Meltzner et al., 2012; Leon et al., 2015). New techniques and measures are needed to build on existing slabbing methods and ensure that representative corals are selected for slabbing.

In this study, we introduce a method to quantitatively document coral surface morphologies in high resolution using two three-dimensional (3D) reconstruction techniques: structure-from-motion (SfM) and LiDAR scans captured with an iPhone. We investigate how this model-based approach differs from more conventional approaches and validate the reconstruction techniques, demonstrating its accuracy in capturing a coral's surface profile. In doing so, we highlight a limitation of the conventional slabbing method. To assess the usefulness of reconstructed 3D models, we then explore practical application of this new approach, utilising the model to enable more rigorous analyses and detailed interpretations of a coral's surface morphology. We also investigate how this model-based approach can complement more conventional field approaches. When applied to multiple corals, this approach can guide the selection of microatolls that are ideal for sampling, ultimately making the slabbing process more efficient. We demonstrate that this method provides important constraints on RSL history where slab extraction is not viable, and, where slabbing is feasible, it can provide crucial details that are not recovered from the slab.

2. Study sites and geological setting

In this study, we applied these 3D reconstruction techniques on fossil coral microatolls from two study sites: 1) Mapur Island, Indonesia, and 2) Paraoir village, Philippines. Corals from these sites were selected due to the availability of photos suitable for 3D reconstruction via SfM photogrammetry. Additionally, the chosen corals have also been slabbed and studied, providing a reference to validate the reconstructed 3D models.

2.1. Mapur Island

Our first study site is on Mapur Island, one of approximately 2000 islands (Hutchinson et al., 2001) in the Riau Islands province on the Sunda Shelf in Indonesia. (Fig. 1). Mapur Island has an area of 40 km^2. The island experiences semi-diurnal tides, with a strong modulation of the tidal range over the 18.6-year nodal tidal cycle [e.g. Haigh et al., 2011; Peng et al., 2019]. Over this tidal cycle, the tidal range varies from 2.33 m to 1.97 m (Majewski, 2017; Egbert and Erofeeva, 2002). The study site is on the southeastern coast of Mapur Island and comprises of a reef flat that gradually deepens into a lagoon farther offshore (Majewski, 2017).

Fieldwork was conducted at Mapur Island from 2012 to 2014. Five fossil microatolls were slabbed and studied in detail (Majewski, 2017), following procedures outlined in Supporting Text S1 (see also Meltzner and Woodroffe, 2015). Of these, four corals (PMPR-B-F2, -F3, -F4 and -F5) had sufficient photos taken in 2012 and 2013 to allow for reconstruction via SfM photogrammetry, although no attempt was made to remove sediments from the coral surface prior to the photo-taking as the photos were not taken with SfM reconstruction in mind. The unremoved sediments included in the images are likely to artificially inflate the elevations derived from the reconstructed 3D model. However, we were unable to revisit the Mapur site to obtain new photographs and therefore utilised existing images for our 3D models.

2.2. Paraoir village

The second study site is Paraoir, situated on the coast of La Union province, Luzon, Philippines. Facing the South China Sea, the site is located approximately 132 km east of the Manila Trench (Sarkawi, 2024) (Fig. 1). Holocene reefs are found on the Paraoir coast (Gong et al., 2012, 2017; Siringan et al., 2016). Paraoir experiences a diurnal

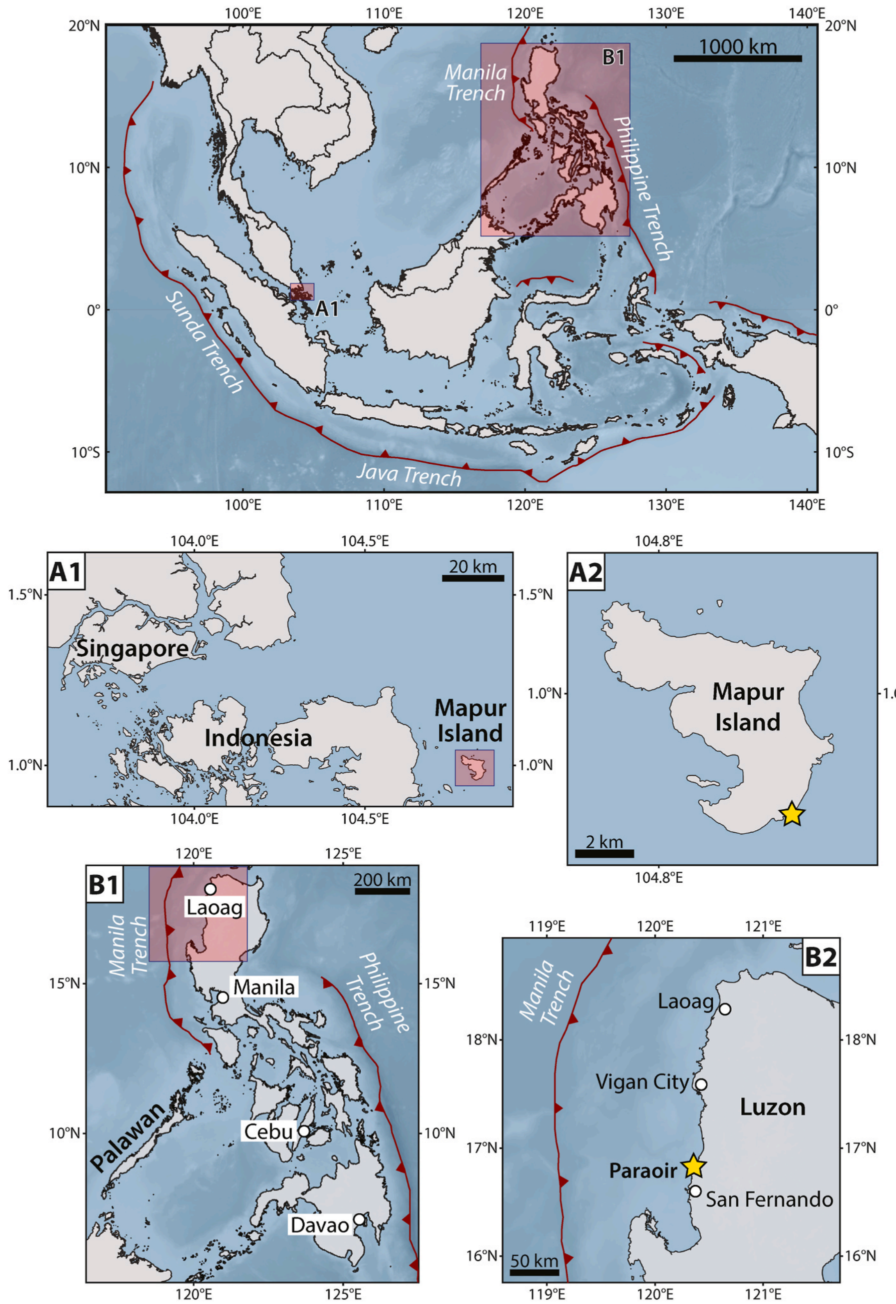

Fig. 1. Map of Southeast Asia and study sites. (A1 and A2) Mapur Island, located within the Riau Islands province, Indonesia. (B1 and B2) Paraoir, a coastal *barangay* (village) in the municipality of Balaoan, La Union province, Philippines. Locations of maps A1 and B1 shown as red boxes in the upper panel; locations of maps A2 and B2 shown as red boxes in panels A1 and A2, respectively. Yellow stars demarcate study sites. Offshore faults and bathymetry from General Bathymetric Chart of the Oceans (GEBCO Compilation Group, 2024).

tidal regime, with a tidal range of 0.65 m between mean low water and mean high water (Sarkawi, 2024).

Most fieldwork was conducted at Paraoir between 2016 and 2018 with four fossil microatolls slabbed in 2018 and studied in detail (Sarkawi, 2024). Since none of the photos taken from 2016 to 2018 were suitable for SfM, we revisited the site in 2022 to obtain new photographs for SfM photogrammetry. We also conducted LiDAR scans with an iPhone 13 Pro. We imaged PARA-F1, a fossil *Porites* sp. coral microatoll with eight visible concentric rings, as it had been slabbed along a complete radius and was accessible (not buried under sand) at the time of our 2022 visit. Photographs of PARA-F1 taken in 2022 inevitably post-dated the slab extraction, which complicated attempts to compare model-derived results directly with the physical slab.

3. Methodology

This section outlines the SfM photogrammetry and iPhone LiDAR scanning techniques, how they were used to generate 3D models of the coral microatolls, and subsequently how we extracted radial information from the final 3D model of a coral. 3D model reconstruction consists of three major steps: (1) preparation for data acquisition, (2) data acquisition, and (3) model ground-truthing.

3.1. Preparation for data acquisition

In preparation for data acquisition, a coral microatoll must be prepared for documentation. Material that has accumulated on the dead surface of the coral, commonly a mixture of sediment, boring mollusks, and plant growth (Fig. S2) (Flora and Ely, 2003; Goreau et al., 1979; Lozano-Cortés and Zapata, 2014), should be removed, particularly from within grooves. Otherwise, such material could fill and mask important features of the surface morphology. Removing this material allows for improved resolution of subtle features on the coral that will be critical for interpretation of the coral growth history. While we were able accomplish this procedure for PARA-F1 during our 2022 site visit, we could not do so for the Mapur corals (PMPR-B-F2, -F3, -F4 and -F5).

3.2. Data acquisition and processing

SfM photogrammetry [e.g. Fonstad et al., 2013; Furukawa and Ponce, 2009; Smith et al., 2015; Snavely et al., 2006] is cost-effective, user-friendly and requires minimal equipment (James et al., 2019; Mosbrucker et al., 2017; Róg and Rzonca, 2021; Westoby et al., 2012). This technique has been used in a range of research topics such as fluvial processes [e.g. Mosbrucker et al., 2017; Dietrich, 2014; Leduc et al., 2019], glacial processes [e.g. Keutterling and Thomas, 2006; Piermattei et al., 2016; Śledź et al., 2021], rock and cliff stability assessments [e.g. Kasprzak et al., 2017; Kong, 2021; Westoby et al., 2018] and storm deposits [e.g. Gienko and Terry, 2013; Sedrati et al., 2022; Vaccher et al., 2023]. In coral studies, 3D models created via SfM photogrammetry are valued for their high accuracy and precision [e.g. Ferrari et al., 2016; Figueira et al., 2015; Rossi et al., 2019], particularly in monitoring coral growth rates and reef morphologies [e.g. Leon et al., 2015; Lange et al., 2022; Raoult et al., 2017]. However, their application in RSL reconstruction using coral microatolls is limited. For instance, Hallmann et al. (2018) used SfM photogrammetry to generate digital elevation models of coral microatolls in the French Polynesian Islands, providing high-resolution site maps and analysis of morphological changes in coral profile. Similarly, Tan et al. (2024) used SfM photogrammetry to supplement drilled coral cores for late-Holocene RSL reconstructions for Singapore.

Airborne and terrestrial LiDAR have separately been used extensively in various fields such as geomorphic surveys [e.g. Bitelli et al., 2000; Roering et al., 2013; Slatton et al., 2007] and fluvial processes [e.g. Bangen et al., 2014; Lohani and Mason, 2001]. iPhone LiDAR, introduced in 2020, features a simplified design using vertical cavity surface emitting laser (VCSEL) emitters and single photon avalanche diode (SPAD) receivers, enabling large-scale, cost-effective production (Chase et al., 2022; King et al., 2022; Losè et al., 2022; Tondo et al., 2023). Since its recent introduction, studies have made use of the iPhone LiDAR's rapid and portable approach, where it has been utilised in studies like forestry mapping [e.g. Gollob et al., 2021; Tatsumi et al., 2022], fluvial studies [e.g. Marshall et al., 2024; Monsalve et al., 2023] and topographic surveys [e.g. Luetzenburg et al., 2021, 2024; Riquelme et al., 2021], but not yet in RSL studies.

We applied SfM photogrammetry to all the corals from Mapur Island and Paraoir village. For SfM photogrammetry, we require a dataset of well-taken (i.e. well-lit, not blurry, not using wide-angle lenses of telephoto function), overlapping photographs (Fig. 2A) (Supporting Text S3.1) (Mosbrucker et al., 2017; Róg and Rzonca, 2021; Iheaturu et al., 2020). These images were processed using a photogrammetric processing software, Agisoft Metashape Professional (version 1.7.2): a stand-alone software product that performs photogrammetric processing of digital images to generate 3D spatial data (Over et al., 2021; Verhoeven, 2011). The model was processed in the following stages: (1) photo alignment, (2) point cloud creation, (3) mesh creation, and (4) georeferencing. The point cloud contains an array of points on the surface, each with coordinates (x, y, z) defining the location of the point in 3D space (Eltner et al., 2016). The points are connected to form a polygonal mesh, which is composed of vertices, edges and faces that define the shape of the reconstructed object (Catalucci et al., 2018; Park and Lee, 2019). Details are in Supporting Text S3.2. For brevity, in this study, we will refer to the mesh and the point cloud collectively as the 3D model, unless specified otherwise.

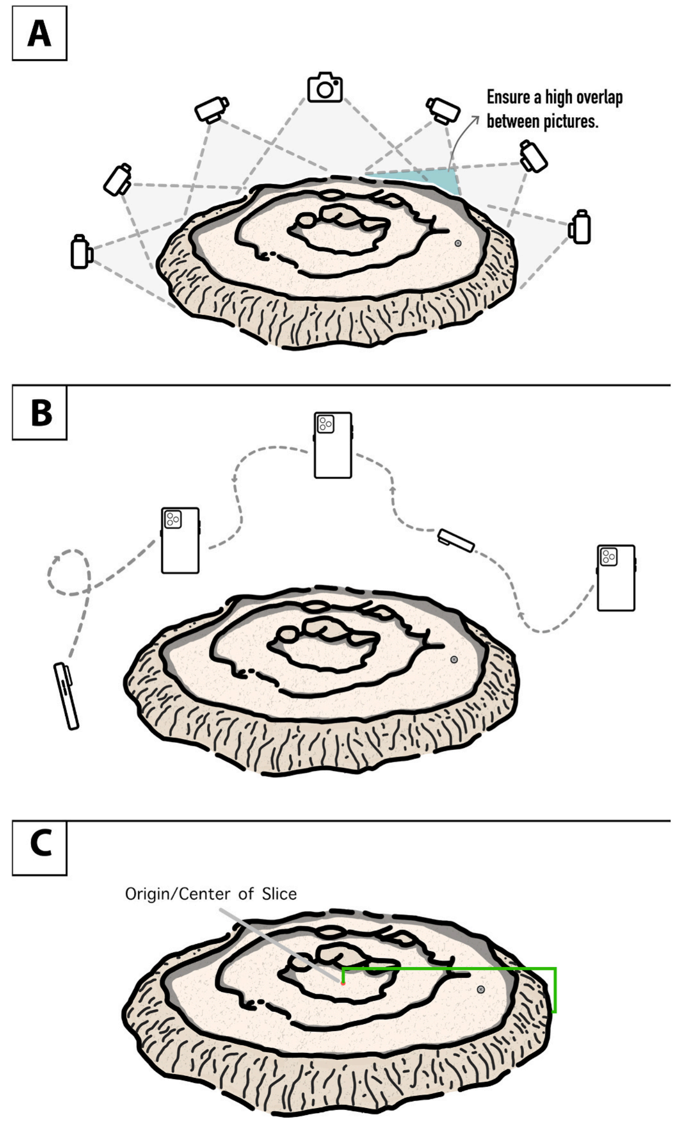

Fig. 2. Simplified illustration of the techniques described in this study. (A) How a photo dataset is acquired for structure-from-motion photogrammetry. Multiple photos of the coral microatoll are taken from different angles and perspectives while ensuring a high overlap between adjacent photos. (B) How a scan is taken using iPhone LiDAR. By walking around the coral and using the iPhone to continuously capture the coral from different angles, the scan can be taken in a short amount of time, while capturing intricate details. (C) Schematic illustration of a slice of the point cloud of a coral. A thin bounding box (green) is projected from the origin point, from which all the points within the confines are sampled.

We also performed iPhone LiDAR scanning on the PARA-F1 coral from Paraoir village. To produce the 3D model of PARA-F1, we utilised the iPhone 13 Pro (released in 2021) and the Scaniverse app, developed by Niantic and initially released in 2021 (Niantic Labs, 2021). The scan is simply performed by walking around the coral with a hand-held iPhone, ensuring that imagery is captured at every angle (Fig. 2B) (Luetzenburg et al., 2021) (Supporting Text S4.1). It is worth noting that although the entire process was accomplished using an iPhone, the same methods can also be performed through an iPad. This technique is particularly suitable for coral microatolls, considering their typical diameter is 3 m or less (Tondo et al., 2023; Luetzenburg et al., 2021; Tamimi, 2022), enabling the scan to be completed within 5–10 min (Tavani et al., 2022), and the model can directly be exported as either a mesh or a point cloud that can be used for further analysis. However, as noted by Luetzenburg et al. (2021) and Tavani et al. (2022), the initial point cloud from the scan is often too sparse to reliably detect features. To address this, we sampled the mesh to create a denser point cloud. We performed this process in CloudCompare (CloudCompare, 2023), an open-source software, and continued with the subsequent processing steps there. Specific steps taken for data processing can be found in Supporting Text S4.2.

3.3. Model ground-truthing

The 3D models created using SfM must be georeferenced; although the images used for SfM photogrammetry inherently contain geolocation information, i.e. from the global positioning system (GPS), their locations lack sufficient accuracy to georeference the resulting 3D model (Ahmed et al., 2022). Therefore, accurate coordinates are necessary for georeferencing the final model.

Separately, while the process of taking an iPhone LiDAR scan inherently involves scaling through direct time-of-flight (dToF) measurements [e.g. Losè et al., 2022; Gollob et al., 2021; Luetzenburg et al., 2021], several studies have highlighted inaccuracies with deviations of up to 10–12 cm [e.g. Losè et al., 2022; Luetzenburg et al., 2021; Łabędź et al., 2022]. However, in Supporting Text S7, we show that iPhone-derived 3D models are scaled accurately, with a maximum deviation of 2.5 cm. While this value is still relatively low, we emphasize the importance of georeferencing with accurate coordinates in ideal scenarios.

Thus, 3D models generated using either method require additional work to ensure proper orientation, scale, and alignment within a global or local coordinate system (Rossi et al., 2019; Sanz-Ablanedo et al., 2018). To scale and locate the 3D models, we selected distinctive points on each coral to be surveyed as ground control points (GCPs). These points were chosen to be evenly distributed across the coral to prevent doming effects in the final model (Supporting Text S5) (Mancini et al., 2017). Each GCP must be carefully photographed and documented so that its location can be accurately identified subsequently in the 3D model. The 3D models were georeferenced to the same coordinate system as the physical slabs to facilitate comparison between the two.

We used the slab, reference, and core screws (Meltzner and Woodroffe, 2015) found on the four fossil corals from Mapur Island to georeference the resulting 3D models, which were created using SfM photogrammetry. Coordinates of each point (relative to a local coordinate system) were surveyed in 2012 and 2013 using a Leica TCRP 1203 total station. All surveyed points were within 100 m of the total station in standard mode; at that range the total station has a stated measurement accuracy of ±1.15 mm. To assess the accuracy of SfM-generated 3D models for Mapur Island, we compared model-predicted coordinates with independent, total-station-derived coordinates of check points (points not used as GCPs) (Supporting Text S6). The low root mean square error (RMSE) values indicated that our reconstructed models accurately represent the coral surface.

In subsequent analysis of PARA-F1, we will be utilising the 3D model created using SfM photogrammetry. Although a model of PARA-F1 was generated using iPhone LiDAR scans, the SfM-derived model was ultimately preferred due to its inherently denser point cloud, a result of the structure-from-motion multi-view-stereo (SfM-MVS) algorithms (Supporting Text S3.2). Moreover, we want to avoid any potential issues associated with the sampling process to obtain a denser iPhone-derived point cloud.

As a total station was not available during the 2022 visit, we could not georeference the resultant model with total-station-derived coordinates. Thus, to georeference the SfM model, coordinates derived from the iPhone LiDAR scan were used as GCPs for georeferencing. This process involves utilising the direct point cloud generated from the iPhone LiDAR scan. Unique and identifiable points that were evenly distributed across the coral surface were identified, and their precise relative coordinates recorded using the "point picking" tool on CloudCompare. Subsequently, these points are identified within the SfM-derived model, and their corresponding iPhone-derived coordinates were inputted as GCPs to georeference the SfM model. Following our findings from Table S5 (Supporting Text S7), we are confident that iPhone-derived coordinates are sufficiently accurate for this step.

3.4. Extraction of information from 3D models for interpretation of coral growth histories

We aim to illustrate the utility of radial profiles of surfaces of the 3D models to aid in the interpretation of coral growth histories. To facilitate this, we developed a method called "slicing", which samples points from the 3D model along a radial profile. A slice consists of a continuous set of measurements along a selected profile (Fig. 2C), similar to the surface profile observed in a physical slab. Slices extracted from the fully 3D model offer key advantages over surface elevation profiles obtained along transects from a 2.5D digital surface model (DSM): DSMs are derived through rasterization to obtain a regular grid output (Guiotte et al., 2019), but this can lead to loss of critical information embedded in the raw point cloud (Guiotte et al., 2020), particularly where higher coral "overhangs" lower coral. Slices in this context should not be confused with physical slices associated with slabbing, which have been discussed in other work [e.g. Meltzner and Woodroffe, 2015]. The process of obtaining a slice starts by locating a point on the coral which will act as the origin of the slice. A thin bounding box is created, which projects outwards from the origin point along the radius of interest. These points are then rotated to the $x-z$ plane to get the corresponding profile. The outcome is a series of continuous points along the chosen radius, representing the surface profile of the coral.

To validate the 3D models' ability to replicate a coral surface morphology with sufficient resolution and accuracy, we will compare the slices from the Mapur corals to the co-located physical slab profiles. Subsequently, we will explore potential advantages and opportunities of the 3D models, using the concentric ring structure of the Mapur and Paraoir coral microatolls and 3D models as examples.

4. Results

For both the Mapur Island and the Paraoir coral microatolls, we developed 3D models and extracted slices from these models. Key results and observations from these models and slices follow below.

4.1. Validation of 3D models against physical slabs: accuracy and sources of discrepancy

We first validated the 3D model approach using the four fossil corals from Mapur Island. From the model for each coral, a slice corresponding to the radius where the physical slab was obtained is extracted via the slicing method. With both the model-derived slice and the physical slab profile in the same reference frame, the two are quantitatively compared, with the slab profile acting as a reference. Details of this procedure are outlined in Supporting Text S8. The mean absolute error (MAE) of the elevation difference between the surface of the physical slab and the co-located model-derived slice, for the four corals, ranged from 5.5 mm to 17.7 mm (Fig. 3). The reasonably low MAE affirms that the 3D models represent the coral surface with reasonable precision. This provides confidence in using the slices for comparisons between different corals at the site, which will be discussed in Section 4.3. However, although the MAE is low, it is not zero. As such, it is helpful to identify the causes of discrepancy between the slab profiles and 3D models, and further investigation is needed for this.

One factor that likely contributes to the discrepancies between the slab profiles and 3D models is that the MAE values calculated from a simple comparison of the slabs and the respective co-located model-derived slices may be biased high by sediment that accumulated in

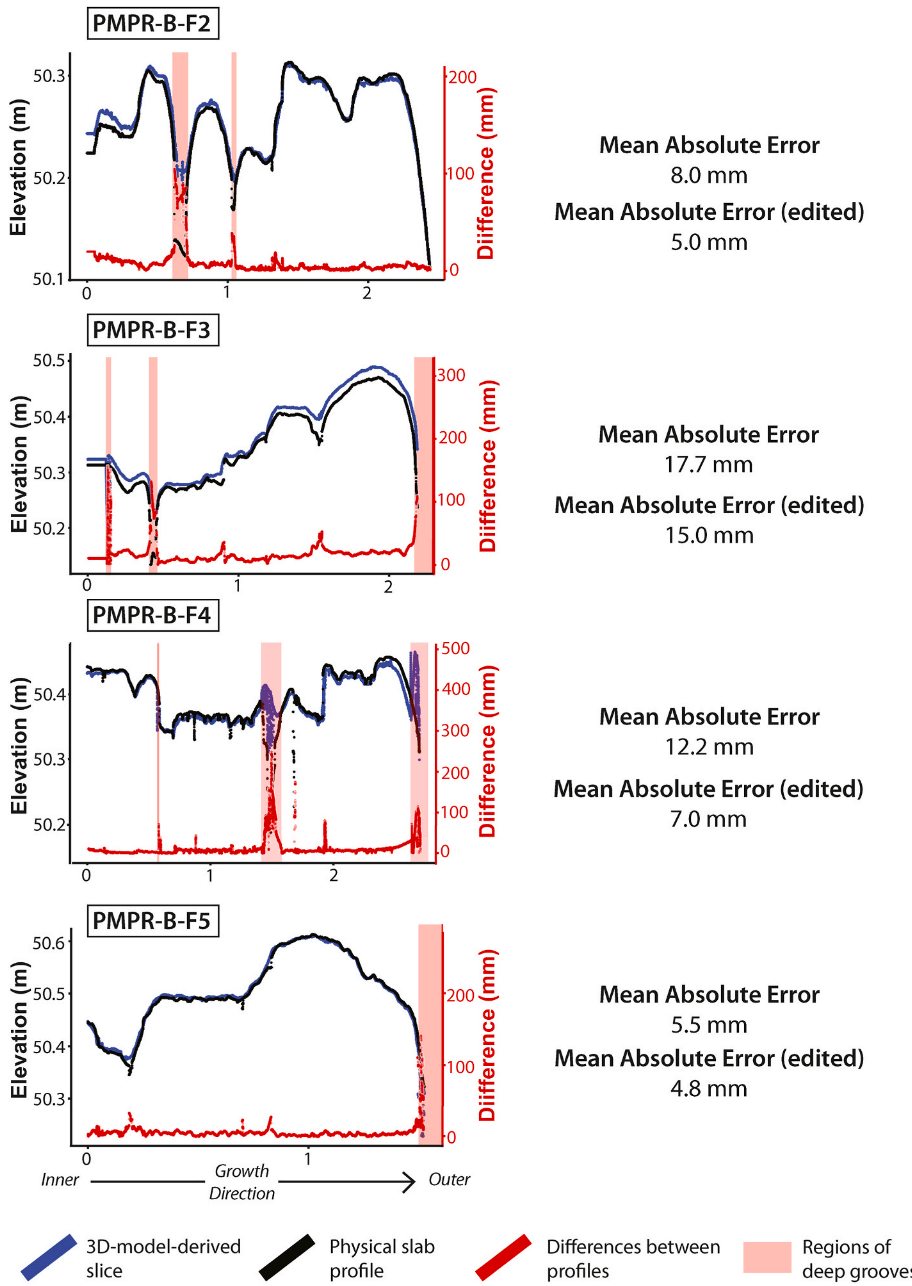

Fig. 3. Comparisons between physical slab profiles and SfM-based model-derived slices. The mean absolute error (MAE) is used to quantify differences between the profiles, where absolute differences are computed at 1 mm intervals. Edited MAE values exclude regions of deep grooves prone to particularly thick sediment accumulation, which can bias the MAE values.

localised deep grooves on the coral (Fig. S2): the sediment was removed during the slabbing process, but it was still included in the photos that were used for the reconstruction via SfM photogrammetry, and was therefore captured in the reconstructed models. We hypothesised that if the thick sediment accumulations had been manually removed prior to the photography, or if we excluded from the comparison any portions of the slab profiles with deep grooves (where thick sediment can accumulate), the agreement between the slabs and slices would improve, an indication that the coral surface is properly represented in the 3D model. Indeed, after excluding those areas, the resulting recalculated differences, termed as "edited differences", were reduced to 4.8–7.0 mm for three out of the four corals examined at the Mapur site (Fig. 3). However, despite this improvement, substantial fractions of the MAE remain.

While some discrepancy could still be attributed to sediment accumulation, it does not appear to explain two cases illustrated in Fig. 3: for the inner (left) portion of the PMPR-B-F2 profile, the model-derived slice is higher, as though tilted, and for the PMPR-B-F3 profile, the model-derived slice is systematically higher than the physical slab. These cases will be discussed in Section 5.3.

4.2. *Interpretation of coral growth history from 3D models of upper surface morphology*

Due to the geometry of the upper surface of a microatoll developing in response to RSL change, the upper surface contains information useful for the reconstruction of RSL. It can be a challenge to fully document the complex geometry of the coral surface, particularly for low-lying corals that may be exposed for only a few hours a month at the lowest tides. However, rapidly acquired 3D models provide a means to obtain data for subsequent analysis. Here we demonstrate some of the critical details pertinent to RSL reconstructions that can be precisely recorded in a 3D model.

An orthomosaic (a top-down, distortion-free image) generated from the 3D model of PARA-F1 (Fig. 4) displays four clearly defined outer concentric rings and four additional, but less distinct, inner rings, all surrounding a lower centre. These eight rings had been identified by researchers in the field prior to slabbing, but they had been documented only in field sketches, photographs, and total station surveys; some important details were not adequately documented during the initial field work in 2016–2018. Using the 3D model developed from field work in 2022, we extracted three full radial slices (A1–A3) to closely examine the outer rings (Figs. 4 and 5A). Adopting the numbering from the slab analysis of Sarkawi (2024), we refer to these as rings R1–R4, with ring numbers increasing inward. From these slices, we observed distinct ring morphologies, with well-defined crests and grooves demarcating rings R1–R4. We note that rings R1–R4 were also distinct in the slab cross section, but evidence for boundaries between rings R5 and R6, and between rings R7 and R8, was not preserved in the slab (Fig. S6). To further assess the ability of the 3D model to characterise rings that are less well-defined, we extracted eight partial slices (B1–B8) through the inner rings (rings R5–R8) of PARA-F1 (Figs. 4 and 5B). While some ring structure was discernible in certain slices (e.g., B1 and B4), this is less apparent in others, and the overall morphology of the inner rings is more subtle.

We focus first on the four clearly defined outer rings, shown as concentric features in the orthomosaic. We aligned radial slices A1–A3 such that ring R3 from each profile overlapped (Fig. 5A). Rings R1–R4 are clearly observed from well-defined ring crests and troughs. In addition to ring identification, the 3D model also allows us to explore relative growth rates. Ideally, corals grow at the same rate over their lifetime, producing concentric rings of identical width and height across all radial profiles. However, natural variability, caused by factors such as environmental stressors or localized disturbances (Lange et al., 2022; Lange and Perry, 2020), often results in slight differences between radii, despite experiencing the same RSL history. These variations can manifest as coeval rings with differing widths across radii. We examined relative growth rates on PARA-F1 by focusing on rings R3 and R4 in the aligned “A” slices (Fig. 5A). The rings on slices A1 and A3 showed similar widths, suggesting comparable growth rates, which is unsurprising due to the proximity of those slices. However, slice A2, located on the opposite side of the coral, revealed some differences. Here, ring R4 appears to be ~50 % thicker than in the other two slices, indicating a faster growth rate at this location. Conversely, ring R3 on slice A2 appears to be ~10 % thinner, suggesting a slowing of the growth rate over time. Further work, such as extracting more slices and aligning profiles more precisely using stretch factors calculated by relative growth rates of coeval rings, can provide insights into the effects of variable growth rates on a single coral. With further analysis, including measurement of ring thickness variability on a sufficient number of radial profiles, a statistical distribution of relative growth rates can be developed, and if average growth rates can be determined by dating the centre and outer edge of the microatoll, or if typical growth rates for the coral genus are known, the relative growth rate distribution can be used to better estimate absolute growth rates.

The 3D models are particularly useful for identifying rings whose boundaries (diedown unconformities) are eroded in cross section, and which are challenging to discern in the field due to overgrowth and/or erosion. For example, ring R7 on PARA-F1, which is not immediately distinguishable from ring R8 in cross section (Fig. S6), is more prominent in slab-adjacent areas (Fig. 4) but harder to locate along other radii. In the orthomosaic, ring R8 is identified by the wide, comparatively flat area in the interior; on the contrary, ring R6 is thinner but elevated (Fig. 6). To scrutinize ring R7 further, we extracted eight partial (not extending the full radius) slice profiles (B1–B8) (Fig. 5B). This ring morphology is most apparent in slices B1 and B8, and to a lesser extent in slices B4 and B5. In slices B2, B6, and B7, ring R7 displays flatter ring morphologies with poorly defined ring crests, suggesting erosion at these locations (Fig. 5B). In contrast, in slice B3, ring R7 seems to be missing, but in its place is an unusually thick ring R6 (Fig. 6). These observations suggest that ring R7 is locally concealed by overgrowth of

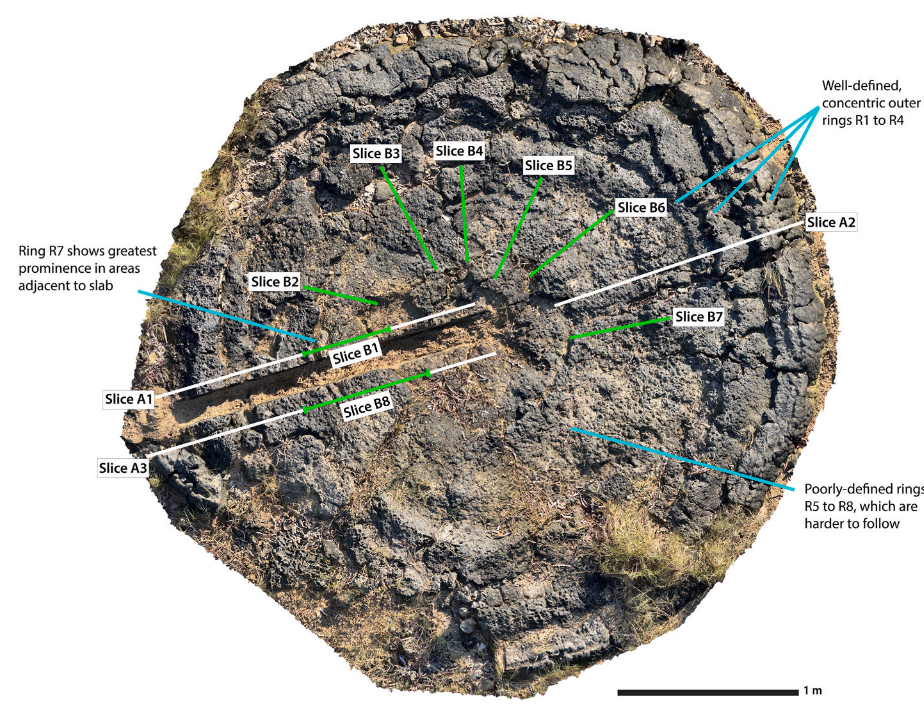

Fig. 4. SfM-based orthomosaic of PARA-F1 showing four clearly defined outer rings (R1-R4), with less defined inner rings (R5-R8). Slices are extracted from the digital 3D model of PARA-F1, to better understand the ring structure of PARA-F1. Each slice is aligned as closely as possible to the coral’s radial growth direction. "A" slices are full radial profiles to examine the outer rings and are shown in Fig. 5A. "B" slices are partial slices that were chosen to highlight spatial variability in ring R7 around the coral and are shown in Fig. 5B.

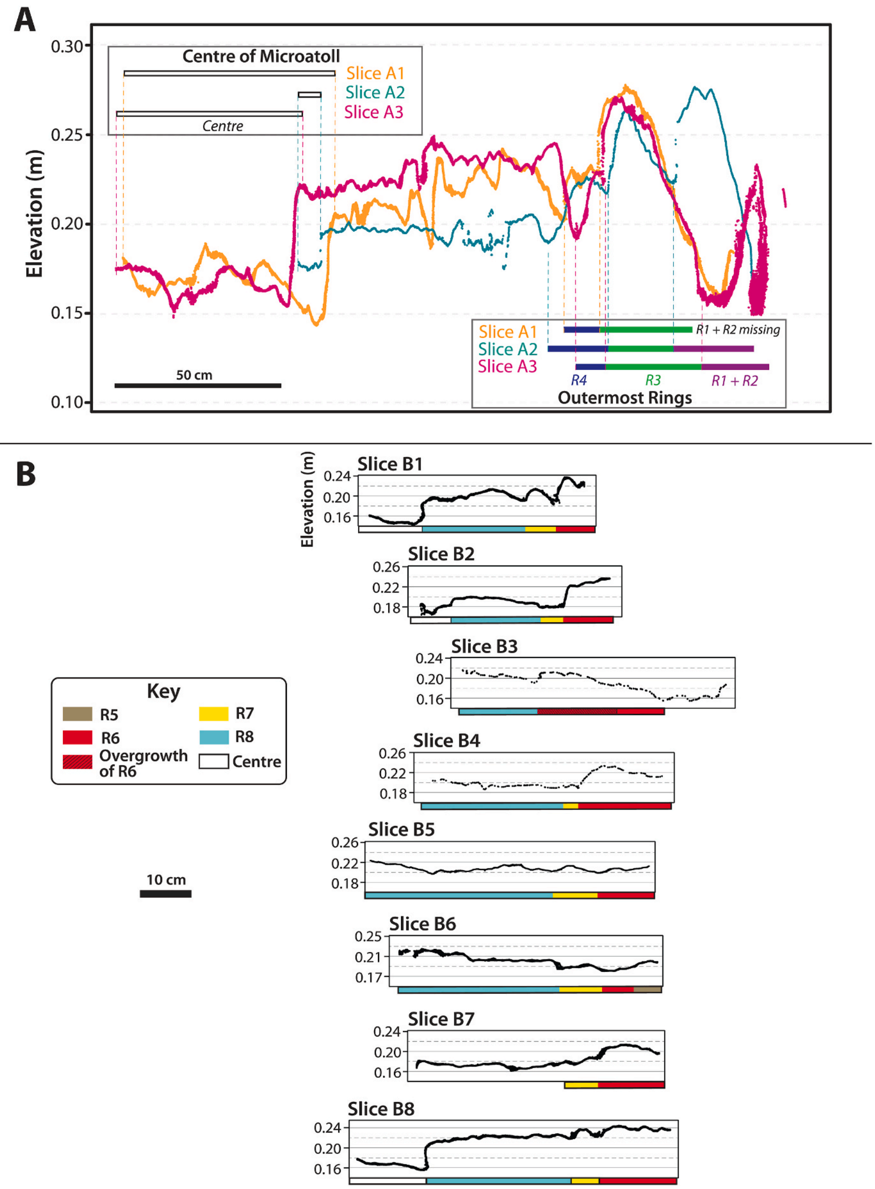

Fig. 5. Quantitative morphological analysis of the SfM-based 3D model from extracted slices of coral microatoll PARA-F1. (A) Comparison of the three full radial slices, A1-A3. Outer rings R1/R2, R3, and R4 are clearly identifiable, and each respective ring exhibits varying widths across the slices, likely reflecting variable growth rates within PARA-F1. In Slice A1, rings R1 and R2 are missing. The sharp decrease in elevation from ring R8 to the centre is also noticeable in all three slices. (B) To study the subtle ring R7, we extracted eight partial slices from the 3D model, where the location of each slice was chosen to verify whether there is ring structure in those locations. A crest and adjacent troughs for ring R7 can be seen in profiles B1, B4, B5 and B8; the ring crest is indistinct in profiles B2, B6 and B7; and the ring is obscured in profile B3. Adjacent rings are indicated by different colours below each profile. The profiles in (A) are vertically exaggerated by a factor of 5.36 for illustrative purposes. The profiles in (B) are plotted with the same horizontal and vertical scale.

the younger ring R6.

4.3. Comparison of potentially coeval microatolls

In the previous section, we demonstrated how slices extracted from a single coral microatoll reveal insights into its ring structure and variable growth rates. Here, we compare slices from multiple coeval corals at a site with variable growth rates, to demonstrate analyses that can be done with 3D models and insights that can be gained.

We utilise PMPR-B-F2, -F4 and -F5, fossil coral microatolls that were previously discussed, to validate the model-based approach. We exclude PMPR-B-F3 from further analysis due to the microatoll being tilted (Majewski, 2017) (Indeed, 3D models are useful for assessing post-growth tilting of a coral microatoll, but that is beyond the scope of the present work.) During initial reconnaissance, it was recognised that PMPR-B-F2 and PMPR-B-F4 belonged to the same population, had compatible but not identical morphologies, and were at similar elevations; based on these observations, it was suspected that the two corals may have been at least partially coeval. In contrast, PMPR-B-F5 grew at a higher elevation and was therefore inferred to be of a different generation. The orthomosaics and slices (Fig. 7) of the three corals support the observations and preliminary interpretations made in the field.

We attempted more rigorous comparisons of the surface morphologies using slices extracted from the 3D models of the respective corals. The outermost ring of PMPR-B-F4 is approximately 15 cm higher than the outermost ring of PMPR-B-F2. However, similarities in the profiles suggest that both corals experienced the same RSL history, despite a small systematic difference in elevation. The two outermost rings, R1 and R2, show similar trends between microatolls, where the increase in elevation from the older R2 to the younger R1 is less than 1 cm on both

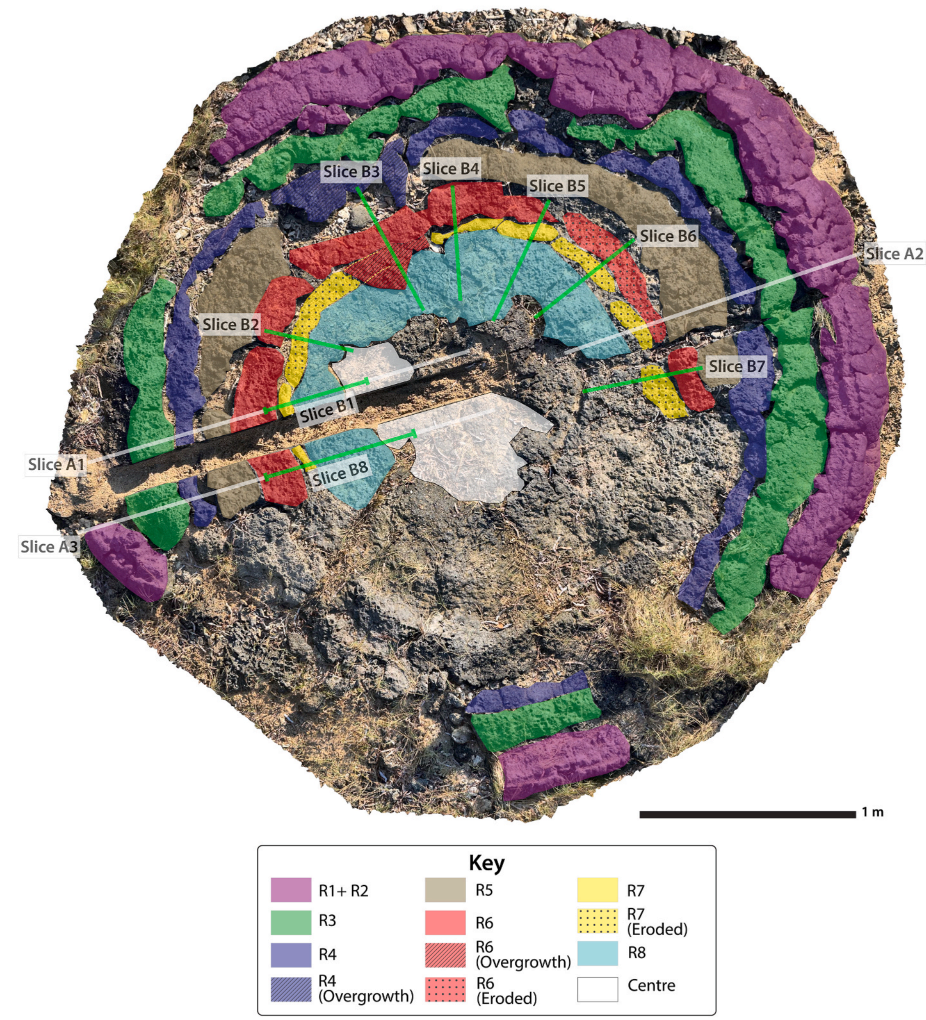

Fig. 6. Orthomosaic of PARA-F1 with interpretations of concentric rings overlain. Relying jointly on the continuity in map view of concentric features and elevation control from the profiles, we can identify the rings, even where moderately eroded, as well as overgrowth. Rings are not indicated where they are severely eroded.

corals. Additionally, we observe similar increases in elevation up to R2: on PMPR-B-F2 we observe an 8-cm increase from older ring R4 to younger ring R2, and on PMPR-B-F4 we observe a 6-cm increase from the flatter surface of older ring R3 to the crest of younger ring R2. The two outermost rings of PMPR-B-F2 are approximately 40 % wider than the seemingly equivalent features on PMPR-B-F4, supporting the suggestion that PMPR-B-F2 and PMPR-B-F4 are coeval, but indicating that they likely grew at different rates. Further analysis such as compiling elevation differences between rings across multiple slice profiles can provide a more representative sampling of ring morphology. This encourages more statistically robust conclusions about coeval rings on a coral.

Comparing PMPR-B-F5 to PMPR-B-F2 and PMPR-B-F4, although the highest ring of PMPR-B-F5 is clearly higher than anything on the other corals, the inner ring of PMPR-B-F5 sits only ~50 mm higher than the outermost ring of PMPR-B-F4 (Fig. 7), suggesting that those rings may be partially coeval but that PMPR-B-F5 may have continued growing after PMPR-B-F2 and PMPR-B-F4 died; this hypothesis could be further tested with radiometric dating. A curious point in the comparison of the potentially coeval rings is that PMPR-B-F2 (the lowest) is the most seaward of the three corals, whereas PMPR-B-F5 (the highest) is the most landward. With only three of the tens of corals at the site fully documented, we can only speculate that the more seaward corals may have settled sometime after death. However, a larger dataset of 3D models and surveyed elevations of microatolls at the site, combined with a few additional radiometric dates, could in theory more conclusively assess whether there are systematic differences across that reef in the elevations of coeval features, which may be consistent with localised slumping.

4.4. Identification of overgrowth

The 3D models developed in this study are particularly useful for comparing radii and identifying overgrowth on coral microatolls — more generally than noted in Section 4.2. When examining different radii of the coral, in-sequence rings can be identified by their symmetry across various radii, where the elevations and widths of coeval rings are approximately similar. These in-sequence rings exhibit continuity in their plane morphology, making them traceable where not eroded or overgrown. In contrast, because overgrowth commonly occurs along some but not all radii of a coral, as was noted on the upper surface of PARA-F1, this characteristic can be useful in helping to recognize overgrowth. Comparing different radii on one or multiple coeval microatolls, overgrowth can be most readily identified by a lack of radial symmetry, i.e., discrepancies in morphology at equivalent points along the radii. If enough radii on a sufficient set of coeval microatolls are examined in detail, some radii are likely to remain free from overgrowth, even where equivalent portions of other radii have a markedly higher ring. Furthermore, if a higher ring is indeed overgrowth, formed from inward growth over the surface of older rings, it should be

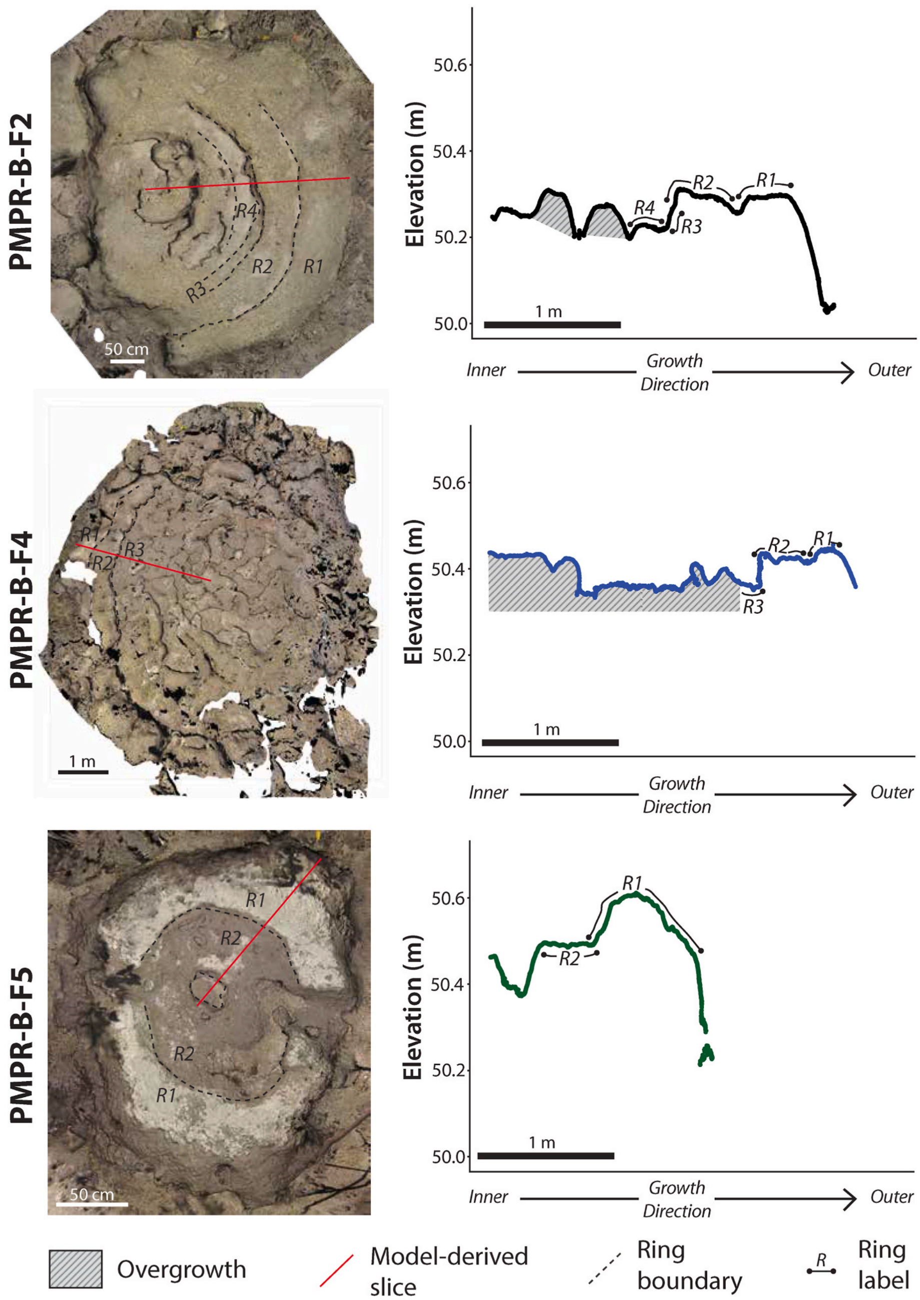

Fig. 7. SfM-based orthomosaics and radial profiles of PMPR-B-F2, PMPR-B-F4, and PMPR-B-F5. The profiles on the right correspond to slices from the same locations where slabs were extracted, indicated with red lines on the corresponding orthomosaics to the left. Rings and overgrowth areas on the slices are labeled based on the ring morphologies identified in the 3D model and field sketches.

morphologically similar to (but a mirror image of) a coeval ring growing outward along the coral's upper surface (Meltzner and Woodroffe, 2015). This is observed on PARA-F1 (Fig. 6), as noted earlier, as well as on PMPR-B-F2 and PMPR-B-F4 (Figs. 7 and 8).

5. Discussion

Details of the coral growth history, particularly in response to RSL change, are preserved on the upper surface of a coral microatoll. If these details can be extracted with sufficient precision and in sufficient resolution, such as in a 3D model derived from SfM or iPhone LiDAR, they can be used to guide RSL reconstructions using coral microatolls.

5.1. Using 3D models to aid in selection of slabbing locations

Slabbing is a demanding, labour-intensive process requiring a dedicated team and careful logistical planning, which can be costly. This motivates efficiency in the collection of slabs that yield valuable information. Preserved diedowns are critical in a slab as they serve as sea-level index points (SLIPs), which have a discrete position of past RSL in space and time (Khan et al., 2019); otherwise, fully eroded diedowns can only be treated as minimum limiting sea-level data (Majewski, 2017). When selecting an optimal location on a microatoll for slabbing, a radius with overgrowth is preferable as the overgrowth can protect underlying rings and diedowns from erosion, promoting the preservation of these features (Meltzner and Woodroffe, 2015). Insights gained from the analysis of 3D models, such as improved ring interpretation and

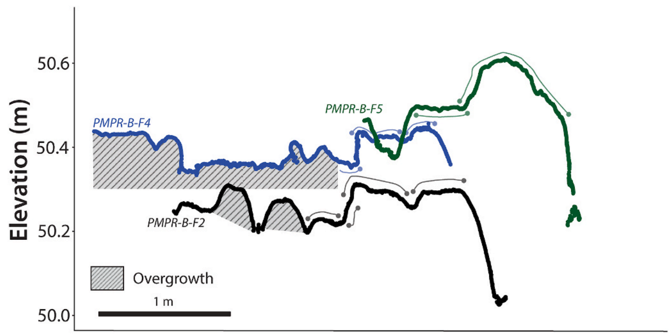

Fig. 8. Inferred chronological alignment of the PMPR-B-F2, PMPR-B-F4 and PMPR-B-F5 slices using information from each slice. The elevation gain from R4 to R2 on PMPR-B-F2 and from R3 to R2 on PMPR-B-F4 are comparable, and the elevation differences between R2 and R1 are also similar on both corals. This consistency suggests that the records from both corals likely overlap. Refer to Fig. 7 for ring labels on each slice.

identification of overgrowth, can streamline this process by guiding the selection of optimal microatolls and optimal radii for slabbing.

Although the location chosen for slabbing of PARA-F1 was reasonably good, we illustrate how a 3D model might have guided us to choose a better radius for slabbing. In the interpreted slab (Fig. S6), the diedown between rings R7 and R8 had been eroded, with only a subtle trough in the coral profile suggesting that a diedown may have occurred. A better location to slab, which cuts through all of the concentric annuli and has a better preserved ring R7, would be near slice B3. The annotated orthomosaic (Fig. 6) shows a thickened R6, which likely results from overgrowth, and which could protect the ring R7 diedown from erosion.

5.2. Maximising information from the coral surface morphology

Even when an optimal radius is chosen for slabbing, it does not necessarily contain complete information. The surface morphology (and hence the 3D model) of a coral microatoll provides quantitative information that is not always preserved in a slab. In addition, the replication of results is critical in science, and 3D models allow for the replication of results from a single coral slab: the 3D models can be used to demonstrate that the RSL history reconstructed from a slab is representative of RSL histories experienced by coeval corals at a site. Finally, in places where coral slab extraction is nonviable, robust RSL histories can be developed using precise observations extracted from 3D models of the coral surfaces. Although RSL histories developed from the surface morphology alone are not as detailed or precise as RSL reconstructed from a slab, they are nonetheless robust and useful.

Returning to the case of PARA-F1, the boundaries between rings R5 and R6 and between R7 and R8 have been eroded in the slab (Fig. S6). Thus, the interpretation of the existence of those rings and the corresponding diedowns depends entirely on an analysis of the coral surface morphology. We can confidently map the rings and overgrowth, and we can quantitatively infer changes in RSL as the coral grew, by identifying concentric rings in the 3D model of the coral; by assessing the continuity of concentric features along different radii; and by measuring the heights and widths, and characterizing crest morphologies, of the concentric rings (Figs. 5 and 6). Replicating such efforts across multiple corals could provide enhanced clarity and more accurate ring identification.

We have illustrated through the Paraoir and Mapur Island examples that information derived from 3D models can support RSL reconstructions. However, it is important to emphasize that this model-based approach is limited to providing details that can be reconstructed or inferred from the coral surface; the internal structure of the coral cannot be entirely resolved. Emerging tools such as Bayesian inversion techniques (Komori et al., 2025) are currently being developed to address this gap.

5.3. "Ground-truthing" physically extracted slabs

In the Mapur case study, small but systematic residuals persisted in some cases when comparing 3D model slices with physical slab profiles, even after excluding areas suspected of significant sediment accumulation. One reason for this minor mismatch could be errors that arise during the slabbing process. During the process of slab extraction, the physical slab is often fragmented; these fragments are subsequently reassembled using an epoxy (Fig. S1) (Meltzner and Woodroffe, 2015), which can introduce minor errors where fragments do not fit perfectly. Additionally, drawing on the line of original horizontality on the slab is another manual process prone to small errors; in this step, surveyed elevations are projected downward from screws inserted into the top of the slab, and a line is traced through the set of projected points (Meltzner and Woodroffe, 2015). Errors can arise due to unavoidable human error, especially if the ruler is not held perfectly perpendicular to the surface (i.e. at an angle). Zachariasen et al. (2000) has demonstrated that errors can emerge when orienting the slab relative to the horizontal, potentially introducing uncertainties in analyses using slab stratigraphy. Among the small set of corals we included in our study, we showed that these errors can accumulate, leading to centimetre-scale or potentially larger inaccuracies. 3D models can be useful in identifying and retrospectively correcting for mistakes commonly made during the slabbing process. Errors that can affect the restoration of horizontality of the slab can result in the slab surface not accurately representing the original coral surface. This seems to have occurred in the case of PMPR-B-F2, where the inner portion of the profile shows the 3D slice to be higher (indicating that the inner half of the slab may have been misaligned), and in the case of PMPR-B-F3, where the 3D slice is systematically higher than the physical slab.

To reconstruct RSL from a coral microatoll, many studies involve the extraction and analysis of a physical slab from the coral. However, until now, there has been no independent way to assess whether the RSL reconstruction is correct, despite the errors that might be introduced in the process, and there is no rigorous, quantitative way to determine whether the RSL history reconstructed from a single microatoll is representative of RSL at the site, despite processes that can affect a coral locally, such as settling or ponding (Meltzner and Woodroffe, 2015).

5.4. Comparison between techniques

In this study, we introduced two techniques for 3D coral microatoll surface reconstruction: SfM photogrammetry and iPhone LiDAR scanning. Both techniques are user-friendly and require far less equipment than slabbing; each has distinct advantages and limitations that users should consider for selecting an appropriate technique. Which method is best in a particular instance depends on the specific requirements of the study and the available resources.

SfM photogrammetry is able to produce high-resolution 3D models (Westoby et al., 2012), allowing finer details such as minute elevation changes to be recorded. To validate the accuracy of SfM-derived models georeferenced with TS coordinates, we identified check points (unique points on the coral surface not used as GCPs) and compared the coordinates derived from the final SfM model to TS-derived coordinates of these check points (Table S3 and Table S4), where low RMSE values give us confidence that SfM-derived metrics are accurate and can be used in further analysis. However, basic training is required to learn how to capture photos effectively (Supporting Text S3.1) for SfM photogrammetry to ensure an accurate, high-quality model. We process the model in Agisoft Metashape Professional (Supporting Text S3.2); added functionality in the Professional version (compared to the free Standard version) allows for the generation of a DEM and orthomosaic (Agisoft LLC, 2021). The Professional version requires a paid license, which may not be accessible to some users. Overall, SfM photogrammetry is best suited for users who have the capacity to process the 3D model and who have access to surveying equipment such as a total station.

iPhone LiDAR scanning offers an equally portable and rapid approach to capturing the coral using structured light. In addition to ease of use, the main advantage of this technique is that there are free applications such as Scaniverse which support iPhone LiDAR scans. Minimal training is needed, as capturing a LiDAR scan is similar to recording a video on a smartphone. To validate the accuracy of iPhone-derived models georeferenced with TS coordinates, we compared model-derived coordinates of known check points against their corresponding TS-derived coordinates (Table S4). Low RMSE values give us confidence that iPhone-derived metrics are accurate and can be used in further analysis. However, the initial point cloud from the iPhone LiDAR scan lacks the density to reliably detect features, necessitating the use of a mesh-derived point cloud for further analysis (Supporting Text S4.2) (Tavani et al., 2022).

More crucially, the main difference between the two techniques lies in the georeferencing step. For SfM-derived models, a final georeferencing step requires coordinate inputs of unique GCPs (Section 3.3). This is due to the geolocation information inherent in the input images lacking sufficient accuracy to georeference the final model (Ahmed et al., 2022). Ideally, the GCP coordinates would be obtained from an elevation survey utilising a total station. In contrast, models generated using iPhone LiDAR scans are inherently scaled using direct time-of-flight measurements. In Table S5, distances between known check points were calculated from direct iPhone-derived models and compared against corresponding distances measured by TS surveys, where we showed the former has sufficient accuracy. This implies that in situations where logistical constraints prevent the use of additional equipment for georeferencing such as a total station, iPhone LiDAR scans are useable as they have inherently accurate scale and orientation, and therefore, can be used in subsequent analyses. Direct iPhone LiDAR scans still require at least one point to be surveyed on the microatoll to place the 3D model in a real-world vertical reference frame, but this can be done at a different time, and it is faster and logistically easier than surveying a full suite of GCPs on a coral, since each survey point must be carefully photographed and documented.

We also take this a step further and demonstrate that in the case of PARA-F1, where a total station survey was not possible on the day of the SfM and iPhone LiDAR acquisitions, a combined approach of leveraging the inherently denser point cloud derived from SfM photogrammetry for model generation and the relative 3D locations of points extracted from the iPhone LiDAR model for georeferencing the SfM model, can yield 3D models with sufficient accuracy and point-cloud density for subsequent analysis.

Ultimately, this model-based approach offers distinct advantages over more traditional slabbing and surveying methods. Beyond its high portability and user-friendliness, model-derived metrics can yield valuable information not easily obtainable through conventional surveying techniques. More crucially, when used to complement slabbing, insights derived from the analysis of one or multiple microatolls can significantly enhance the efficiency and robustness of the slabbing process.

6. Conclusions

This study introduces the use of SfM photogrammetry and iPhone LiDAR scans as fast, user-friendly techniques for generating detailed 3D models of coral microatolls. Data extracted from the 3D models can be used in further RSL studies, to improve the effectiveness and replicability of coral microatolls as a geological proxy, and to allow microatolls to be utilised in RSL studies more broadly. We begin by validating this model-based approach, assessing the precision and resolution of the 3D models, and emphasising the importance of cleaning the coral to increase the accuracy of the model results.

While slabbing remains the preferred method for reconstructing RSL due to its ability to reveal the internal structure of a coral microatoll, it can be difficult to determine whether selected slabs will yield representative and complete RSL records. 3D models can address these limitations by enabling more detailed examinations and quantitative comparisons of the surface morphologies of multiple coral microatolls at a site. This information can guide decisions on which corals are most valuable to slab at a site and allows researchers to identify the most suitable locations on a coral for slabbing. We hope to integrate model-derived data with more statistical tools to maximise the application of 3D models, thereby promoting data collection and analysis efforts by researchers utilising coral microatolls.

CRediT authorship contribution statement

Nurul Syafiqah Tan: Writing – review & editing, Writing – original draft, Methodology, Formal analysis, Conceptualization. **Rohan Gautam:** Writing – review & editing, Software, Methodology. **Fangyi Tan:** Writing – review & editing. **Gina M. Sarkawi:** Writing – review & editing, Resources. **Jędrzej M. Majewski:** Writing – review & editing, Resources. **Junki Komori:** Writing – review & editing. **Shi Jun Wee:** Writing – review & editing, Methodology. **Khai Ken Leoh:** Writing – review & editing, Methodology. **Lucas D. Koh:** Writing – review & editing, Methodology. **Adam D. Switzer:** Writing – review & editing, Funding acquisition. **Aron J. Meltzner:** Writing – review & editing, Writing – original draft, Supervision, Project administration, Funding acquisition, Conceptualization.

Data statement

Source data and code used in this paper.

Data	Source
Point clouds of the Mapur Island and Paraoir corals	https://doi.org/10.5281/zenodo.17140808
Code for slice extraction	https://doi.org/10.5281/zenodo.14049212

Declaration of competing interest

The authors declare that they have no known competing financial interests or personal relationships that could have appeared to influence the work reported in this paper.

Acknowledgements

This work was primarily supported by the National Research Foundation (NRF) Singapore under its Singapore NRF Fellowship scheme (Award NRF-NRFF11-2019-0008 to AJM). This research was also supported by the Singapore Ministry of Education (MOE) Academic Research Fund (Award MOE2019-T3-1-004) and the National Research Foundation (NRF) Singapore and the Singapore Ministry of Education (MOE) under the Research Centres of Excellence initiative. J.M. Majewski is supported by project No. 2022/47/P/ST10/02329 co-funded by the National Science Centre and the European Union's Horizon 2020 research and innovation programme under the Marie Skłodowska-Curie grant agreement No. 945339. We are grateful for the help of many colleagues who provided advice based on expert observations, including L.T. Aung, J. Quye-Sawyer, W.L. Neo, and J.Y. Yeo., and we are thankful to the numerous undergraduates in the Asian School of the Environment at Nanyang Technological University who provided feedback on the workflow. We also thank D.H. Natawidjaja, B.W. Suwargadi, I. Suprihanto, and D. Prayudi for logistics and field support in Indonesia, and N.T. Ramos, R. Cortez, L. Tiston, G. Quina, G. Tiston, L.W. Orsolina, D. Prayudi, and Amar for logistics and field support in the Philippines.

We thank the residents of P. Mapur in Indonesia and Brgy. Paraoir in the Philippines for allowing us to conduct field work on their land. We thank Rich Briggs and an anonymous reviewer for their constructive feedback, which greatly improved this manuscript. This paper and the methods described herein were developed primarily during field work in Singapore, research that was conducted under the Singapore National Parks Board research permit NP/RP20-122, with support of the Sentosa Development Corporation team, particularly G. Lee, L. Tan, and the Sentosa environmental management team. This is Earth Observatory of Singapore contribution no. 630.

Appendix A. Supplementary data

Supplementary data to this article can be found online at https://doi.org/10.1016/j.srs.2025.100288.

Data availability

Source data and the code used are provided with this paper.

References

Agisoft LLC, 2021. Agisoft Metashape User Manual, Professional Edition, Version 1.7. https://www.agisoft.com/pdf/metashape-pro_1_7_en.pdf. (Accessed 15 October 2024).

Ahmed, S., El-Shazly, A., Abed, F., Ahmed, W., 2022. The influence of flight direction and camera orientation on the quality product of UAV-based SfM-photogrammetry. Appl. Sci. 12 (20), 10492. https://doi.org/10.3390/app122010492.

Bangen, S.G., Wheaton, J.M., Bouwes, N., Bouwes, B., Jordan, C., 2014. A methodological intercomparison of topographic survey techniques for characterizing wadeable streams and rivers. Geomorphology 206, 343–361. https://doi.org/10.1016/j.geomorph.2013.10.010.

Bitelli, G., Dubbini, M., Zanutta, A., 2000. Terrestrial Laser Scanning and digital photogrammetry techniques to monitor landslide bodies. In: Altan, O. (Ed.), ISPRS Archives – Volume XXXV Part B5, 2004, 12-23 July 2004, pp. 246–251. Istanbul Turkey. https://www.isprs.org/proceedings/xxxv/congress/comm5/papers/558.pdf.

Camoin, G.F., Webster, J.M., 2015. Coral reef response to Quaternary sea-level and environmental changes: state of the science. Sedimentology 62 (2), 401–428. https://doi.org/10.1111/sed.12184.

Catalucci, S., Marsili, R., Moretti, M., Rossi, G., 2018. Comparison between point cloud processing techniques. Measurement 127, 221–226. https://doi.org/10.1016/j.measurement.2018.05.111.

Chase, P., Clarke, K., Hawkes, A., Jabari, S., Jakus, J., 2022. Apple IPhone 13 Pro LiDAR accuracy assessment for engineering applications. 2022: the Digital Reality of Tomorrow, 23-25 August 2022, Fredericton, New Brunswick, Canada. University of New Brunswick Libraries. https://doi.org/10.57922/tcrc.645.

Clark, J.A., Farrell, W.E., Peltier, W.R., 1978. Global changes in postglacial sea level: a numerical calculation. Quat. Res. 9 (3), 265–281. https://doi.org/10.1016/0033-5894(78)90033-9.

Clark, P.U., Dyke, A.S., Shakun, J.D., Carlson, A.E., Clark, J., Wohlfarth, B., Mitrovica, J. X., Hostetler, S.W., McCabe, A.M., 2009. The last glacial maximum. Science 325 (5941), 710–714. https://doi.org/10.1126/science.1172873.

CloudCompare (version 2.12), 2023. 3D point cloud and mesh processing software. http://www.cloudcompare.org/.

Dietrich, J.T., 2014. Applications of Structure-From-Motion Photogrammetry to Fluvial Geomorphology. Ph.D. thesis, University of Oregon, 1794/18701.

Egbert, G.D., Erofeeva, S.Y., 2002. Efficient inverse modeling of barotropic ocean tides. AMETSOC 19 (2), 183–204. https://doi.org/10.1175/1520-0426(2002)019.

Eltner, A., Kaiser, A., Castillo, C., Rock, G., Neugirg, F., Abellán, A., 2016. Image-based surface reconstruction in geomorphometry – merits, limits and developments. Earth Surf. Dyn. 4 (2), 359–389. https://doi.org/10.5194/esurf-4-359-2016.

Ferrari, R., McKinnon, D., He, H., Smith, R.N., Corke, P., González-Rivero, M., Mumby, P. J., Upcroft, B., 2016. Quantifying multiscale habitat structural complexity: a cost-effective framework for underwater 3D modelling. Remote Sens. 113. https://doi.org/10.3390/rs8020113.

Figueira, W., Ferrari, R., Weatherby, E., Porter, A., Hawes, S., Byrne, M., 2015. Accuracy and precision of habitat structural complexity metrics derived from underwater photogrammetry. Remote Sens. 7 (12), 16883–16900. https://doi.org/10.3390/rs71215859.

Fleming, K., Johnston, P., Zwartz, D., Yokoyama, Y., Lambeck, K., Chappell, J., 1998. Refining the eustatic sea-level curve since the Last Glacial Maximum using far- and intermediate-field sites. Earth Planet Sci. Lett. 163 (1–4), 327–342. https://doi.org/10.1016/s0012-821x(98)00198-8.

Flora, C.J., Ely, P.S., 2003. Surface growth rings of Porites lutea microatolls accurately track their annual growth. Northwest Sci. 77 (3), 237–245. https://hdl.handle.net/2376/798.

Fonstad, M., Dietrich, J.T., Courville, B.C., Jensen, J.L., Carbonneau, P.E., 2013. Topographic structure from motion: a new development in photogrammetric measurement. Earth Surf. Process. Landf. 38 (4), 421–430. https://doi.org/10.1002/esp.3366.

Furukawa, Y., Ponce, J., 2009. Accurate, dense, and robust multiview stereopsis. IEEE Trans. Pattern Anal. Mach. Intell. 32 (8), 1362–1376. https://doi.org/10.1109/TPAMI.2009.161.

GEBCO Compilation Group, 2024. GEBCO 2024 Grid. https://doi.org/10.5285/1c44ce99-0a0d-5f4f-e063-7086abc0ea0f.

Gehrels, R., Long, A., 2008. Sea level is not level: the case for a new approach to predicting UK sea-level rise. Geography 93 (1), 11–16. https://doi.org/10.1080/00167487.2008.12094214.

Gienko, G.A., Terry, J.P., 2013. Three-dimensional modeling of coastal boulders using multi-view image measurements. Earth Surf. Process. Landf. 39 (7), 853–864. https://doi.org/10.1002/esp.3485.

Gollob, C., Ritter, T., Kraßnitzer, R., Tockner, A., Nothdurft, A., 2021. Measurement of forest inventory parameters with apple iPad Pro and integrated LiDAR Technology. Remote Sens. 13 (16), 3129. https://doi.org/10.3390/rs13163129.

Gong, S.-Y., Wu, T.-R., Siringan, F.P., Lin, K., Shen, C.C., 2012. An abrupt backreef infilling in a Holocene reef, Paraoir, Northwestern Luzon, Philippines. Coral Reefs 32 (1), 293–303. https://doi.org/10.1007/s00338-012-0982-0.

Gong, S.-Y., Li, H.-C., Siringan, F.P., Zhao, M., Kang, S.-C., Chou, C.-Y., 2017. AMS Carbon-14 dating of microbial carbonates in Holocene coral reefs, Western Luzon, Philippines. Quat. Int. 447, 27–34. https://doi.org/10.1016/j.quaint.2017.06.015.

Goodwin, I.D., Harvey, N., 2008. Subtropical sea-level history from coral microatolls in the Southern Cook Islands, since 300 AD. Mar. Geol. 253 (1–2), 14–25. https://doi.org/10.1016/j.margeo.2008.04.012.

Goreau, T.F., Goreau, N.I., Goreau, T.J., 1979. Corals and coral reefs. Sci. Am. 241 (2), 124–137. http://www.jstor.org/stable/24965267.

Guiotte, F., Lefèvre, S., Corpetti, T., 2019. Rasterization strategies for airborne LiDAR classification using attribute profiles. In: 2019 Joint Urban Remote Sensing Event (JURSE), pp. 1–4. https://doi.org/10.1109/JURSE.2019.8808945. *22-24 May 2019, Vannes, France*.

Guiotte, F., Pham, M.-T., Dambreville, R., Corpetti, T., Lefèvre, S., 2020. Semantic segmentation of LiDAR points clouds: rasterization beyond digital elevation models. IEEE Geoscience and Remote Sensing Letters 17 (11), 2016–2019. https://doi.org/10.1109/lgrs.2019.2958858.

Haigh, I.D., Eliot, M., Pattiaratchi, C., 2011. Global influences of the 18.61 year nodal cycle and 8.85 year cycle of lunar perigee on high tidal levels. J. Geophys. Res. Atmos. 116 (C6). https://doi.org/10.1029/2010jc006645.

Hallmann, N., Camoin, G.A., Eisenhauer, A., Botella, A., Milne, G.A., Vella, C., Samankassou, E., Pothin, V., Dussouillez, P., Fleury, J., Fietzke, J., 2018. Ice volume and climate changes from a 6000 year sea-level record in French Polynesia. Nat. Commun. 9 (1). https://doi.org/10.1038/s41467-017-02695-7.

Hutchinson, F.E., Negara, S.D., 2001. Situating the Riau islands. In: Hutchinson, F.E., Negara, S.D. (Eds.), The Riau Islands: Setting Sail. ISEAS – Yusof Ishak Institute, Singapore, pp. 5–16.

Iheaturu, C.J., Ayodele, E.G., Okolie, C.J., 2020. An assessment of the accuracy of structure-from-motion (SfM) photogrammetry for 3D terrain mapping. Geomatics, Landmanagement and Landscape 2, 65–82. https://doi.org/10.15576/gll/2020.2.65.

James, M.R., Chandler, J.H., Eltner, A., Miller, P.E., Mills, J.P., Noble, T., Robson, S., Lane, S.N., 2019. Guidelines on the use of structure-from-motion photogrammetry in geomorphic research. Earth Surf. Process. Landf. 44 (10), 2081–2084. https://doi.org/10.1002/esp.4637.

Kasprzak, M., Jancewicz, K., Michniewicz, A., 2017. UAV and SfM in detailed Geomorphological mapping of granite tors: an example of starościńskie Skały (sudetes, SW Poland). Pure Appl. Geophys. 175 (9), 3193–3207. https://doi.org/10.1007/s00024-017-1730-8.

Kelsey, H.M., Engelhart, S.E., Pilarczyk, J.E., Horton, B.P., Rubin, C., Daryono, M., Ismail, N., Hawkes, A.D., Bernhardt, C.E., Cahill, N., 2015. Accommodation space, relative sea level, and the archiving of paleo-earthquakes along subduction zones. Geology 43 (8), 675–678. https://doi.org/10.1130/g36706.1.

Kemp, A.C., Hawkes, A.D., Donnelly, J.P., Vane, C.H., Horton, B.P., Hill, T.D., Anisfield, S.C., Parnell, A.C., Cahill, N., 2015. Relative sea-level change in Connecticut (USA) during the last 2200 yrs. Earth Planet Sci. Lett. 428, 217–229. https://doi.org/10.1016/j.epsl.2015.07.034.

Keutterling, A., Thomas, A., 2006. Monitoring glacier elevation and volume changes with digital photogrammetry and GIS at Gepatschferner glacier, Austria. Int. J. Rem. Sens. 27 (19), 4371–4380. https://doi.org/10.1080/01431160600851819.

Khan, N.S., Ashe, E., Shaw, T.A., Vacchi, M., Walker, J., Peltier, W.R., Kopp, R.E., Horton, B.P., 2015. Holocene relative seasea-level changes from near-, intermediate-, and far-field locations. Curr. Clim. Change Rep. 1 (4), 247–262. https://doi.org/10.1007/s40641-015-0029-z.

Khan, N.S., Horton, B.P., Engelhart, S., Rovere, A., Vacchi, M., Ashe, E.L., Törnqvist, T.E., Dutton, A., Hijma, M.P., Shennan, I., 2019. Inception of a global atlas of sea levels since the Last Glacial Maximum. Quat. Sci. Rev. 220, 359–371. https://doi.org/10.1016/j.quascirev.2019.07.016.

King, F., Kelly, R., Fletcher, C.G., 2022. Evaluation of LIDAR-Derived snow depth estimates from the iPhone 12 Pro. IEEE Geoscience and Remote Sensing Letters 19, 1–5. https://doi.org/10.1109/lgrs.2022.3166665.

Komori, J., Gautam, R., Tan, N.S., Meltzner, A.J., 2025. Simulation-based approach for reconstructing past relative seasea-level changes using coral microatolls. Geomorphology 473, 109609. https://doi.org/10.1016/j.geomorph.2025.109609.

Kong, X., 2021. Identifying geomorphological changes of coastal cliffs through point cloud registration from UAV images. Remote Sens. 13 (16), 3152. https://doi.org/10.3390/rs13163152.

Łabędź, P., Skabek, K., Ozimek, P., Rola, D., Ozimek, A., Ostrowska, K., 2022. Accuracy verification of surface models of Architectural objects from the iPad LiDAR in the context of photogrammetry methods. Sensors 22 (21), 8504. https://doi.org/10.3390/s22218504.

Labs, Niantic, 2021. Niantic acquires Scaniverse to power AR mapping and tools. https://nianticlabs.com/news/scaniverse?hl=en. (Accessed 12 September 2024).

Lambeck, K., Rouby, H., Purcell, A., Sambridge, M., 2014. Sea level and global ice volumes from the last glacial maximum to the Holocene. Proc. Natl. Acad. Sci. 111 (43), 15296–15303. https://doi.org/10.1073/pnas.1411762111.

Lange, I.D., Perry, C.T., 2020. A quick, easy and non-invasive method to quantify coral growth rates using photogrammetry and 3D model comparisons. Methods Ecol. Evol. 11 (6), 714–726. https://doi.org/10.1111/2041-210X.13388.

Lange, I.D., Molina-Hernández, A., Medellín-Maldonado, F., Perry, C.T., Álvarez-Filip, L., 2022. Structure-from-motion photogrammetry demonstrates variability in coral growth within colonies and across habitats. PLoS One 17 (11), e0277546. https://doi.org/10.1371/journal.pone.0277546.

Leduc, P., Peirce, S., Ashmore, P., 2019. Short communication: challenges and applications of structure-from-motion photogrammetry in a physical model of a braided river. Earth Surf. Dyn. 7 (1), 97–106. https://doi.org/10.5194/esurf-7-97-2019.

Leon, J.X., Roelfsema, C.F., Saunders, M.I., Phinn, S.R., 2015. Measuring coral reef terrain roughness using 'Structure-from-Motion' close-range photogrammetry. Geomorphology 242, 21–28. https://doi.org/10.1016/j.geomorph.2015.01.030.

Li, T., Chua, S., Tan, F., Khan, N.S., Shaw, T.A., Majewski, J., Meltzner, A.J., Switzer, A. D., Wu, P., Horton, B.P., 2023. Glacial isostatic adjustment modelling of the mid-holocene sea-level highstand of Singapore and Southeast Asia. Quat. Sci. Rev. 319, 108332. https://doi.org/10.1016/j.quascirev.2023.108332.

Lohani, B., Mason, D.C., 2001. Application of airborne scanning laser altimetry to the study of tidal channel geomorphology. ISPRS J. Photogrammetry Remote Sens. 56 (2), 100–120. https://doi.org/10.1016/s0924-2716(01)00041-7.

Losè, L.T., Spreafico, A., Chiabrando, F., Tonolo, F.G., 2022. Apple LiDAR sensor for 3D surveying: tests and results in the cultural heritage domain. Remote Sens. 14 (17), 4157. https://doi.org/10.3390/rs14174157.

Lozano-Cortés, D.F., Zapata, F.A., 2014. Invertebrate colonization on artificial substrates in a coral reef at Gorgona Island, Colombian Pacific Ocean. Rev. Biol. Trop. 62 (1), 161–168. https://doi.org/10.15517/rbt.v62i0.16273.

Luetzenburg, G., Kroon, A., Bjørk, A.A., 2021. Evaluation of the Apple iPhone 12 Pro LIDAR for an application in geosciences. Sci. Rep. 11 (1). https://doi.org/10.1038/s41598-021-01763-9.

Luetzenburg, G., Kroon, A., Kjeldsen, K.K., Splinter, K.D., Bjørk, A.A., 2024. High-resolution topographic surveying and change detection with the iPhone LiDAR. Nature Protocols. 19, 3520-3541. https://doi.org/10.1038/s41596-024-01024-9.

Majewski, J.M., 2017. Coral Microatoll Based Sea Level Records from the Sunda Shelf. Ph.D. thesis. Nanyang Technological University. doi:10.32657/10356/73241.

Majewski, J.M., Meltzner, A.J., Switzer, A.D., Shaw, T.A., Li, T., Bradley, S., Walker, J.S., Kopp, R.E., Samanta, D., Natawidjaja, D.H., Suwargadi, B.W., Horton, B.P., 2022. Extending instrumental Sea-Level records using coral microatolls, an example from Southeast Asia. Geophys. Res. Lett. 49, e2021GL095710. https://doi.org/10.1029/2021gl095710.

Mancini, F., Castagnetti, C., Rossi, P., Dubbini, M., Fazio, N.L., Perrotti, M., Lollino, P., 2017. An integrated procedure to assess the stability of coastal rocky cliffs: from UAV Close-Range photogrammetry to geomechanical finite element modeling. Remote Sens. 9 (12), 1235. https://doi.org/10.3390/rs9121235.

Marshall, A., Morrison, R.R., Jones, B., Triantafillou, S., Wohl, E., 2024. Handheld lidar as a tool for characterizing wood-rich river corridors. River Res. Appl. 40 (3), 353–364. https://doi.org/10.1002/rra.4239.

Meltzner, A.J., Sieh, K., Chiang, H.-W., Shen, C.-C., Suwargadi, B.W., Natawidjaja, D.H., Philibosian, B.E., Briggs, R.W., Galetzka, J., 2010. Coral evidence for earthquake recurrence and an A.D. 1390-1455 cluster at the south end of the 2004 Aceh-Andaman rupture. J. Geophys. Res. 115, B10402. https://doi.org/10.1029/2010JB007499.

Meltzner, A.J., Sieh, K., Chiang, H.-W., Shen, C.-C., Suwargadi, B.W., Natawidjaja, D.H., Philibosian, B.E., Briggs, R.W., 2012. Persistent temini of 2004- and 2005-like ruptures of the Sunda megathrust. J. Geophys. Res. 117, B04405. https://doi.org/10.1029/2011JB008888.

Meltzner, A.J., Woodroffe, C.D., 2015. Coral microatolls. In: Shennan, I., Long, A.J., Horton, B.P. (Eds.), Handbook of Sea-Level Research. John Wiley & Sons, UK, pp. 125–145. https://doi.org/10.1002/9781118452547.ch8.

Meltzner, A.J., Switzer, A.D., Horton, B.P., Ashe, E., Qiu, Q., Hill, D.F., Bradley, S.L., Kopp, R.E., Hill, E.M., Majewski, J.M., Natawidjaja, D.H., Suwargadi, B.W., 2017. Half-metre sea-level fluctuations on centennial timescales from mid-Holocene corals of Southeast Asia. Nat. Commun. 8 (14387). https://doi.org/10.1038/ncomms14387.

Milne, G.A., Mitrovica, J.X., 2008. Searching for eustasy in deglacial sea-level histories. Quat. Sci. Rev. 27 (25–26), 2292–2302. https://doi.org/10.1016/j.quascirev.2008.08.018.

Mitrovica, J.X., Milne, G.A., 2002. On the origin of late Holocene sea-level highstands within equatorial ocean basins. Quat. Sci. Rev. 21 (20–22), 2179–2190. https://doi.org/10.1016/s0277-3791(02)00080-x.

Mitrovica, J., Gomez, N., Morrow, E., Hay, C., Latychev, K., Tamisiea, M.E., 2011. On the robustness of predictions of sea level fingerprints. Geophys. J. Int. 187 (2), 729–742. https://doi.org/10.1111/j.1365-246x.2011.05090.x.

Mix, A.C., Bard, E., Schneider, R., 2001. Environmental processes of the ice age: land, oceans, glaciers (EPILOG). Quat. Sci. Rev. 20 (4), 627–657. https://doi.org/10.1016/s0277-3791(00)00145-1.

Miyata, T., Maeda, Y., Matsumoto, E., Matsushima, Y., Rodda, P., Sugimura, A., Kayanne, H., 1990. Evidence for a Holocene high sea-level stand, vanua levu, Fiji. Quat. Res. 33 (3), 352–359. https://doi.org/10.1016/0033-5894(90)90061-o.

Monsalve, A., Yager, E.M., Tonina, D., 2023. Evaluating Apple iPhone LiDAR measurements of topography and roughness elements in coarse bedded streams. Journal of Ecohydraulics 10 (2), 181–191. https://doi.org/10.1080/24705357.2023.2204087.

Mosbrucker, A.R., Major, J.J., Spicer, K.R., Pitlick, J., 2017. Camera system considerations for geomorphic applications of SfM photogrammetry. Earth Surf. Process. Landf. 42 (6), 969–986. https://doi.org/10.1002/esp.4066.

Natawidjaja, D.H., Sieh, K., Ward, S.N., Cheng, H., Edwards, L., Galetzka, J., Suwargadi, B.W., 2004. Paleogeodetic records of seismic and aseismic subduction from central Sumatran microatolls, Indonesia. J. Geophys. Res. Atmos. 109 (B4). https://doi.org/10.1029/2003jb002398.

Over, J.R., Ritchie, A.C., Kranenburg, C.J., Brown, J.A., Buscombe, D., Noble, T., Sherwood, C.R., Warrick, J.A., Wernette, P.A., 2021. Processing Coastal Imagery with Agisoft Metashape Professional Edition, Version 1.6—Structure from Motion Workflow Documentation. U.S. Geological Survey Open-File Report 2021–1039, p. 46. https://doi.org/10.3133/ofr20211039.

Park, H., Lee, D., 2019. Comparison between point cloud and mesh models using images from an unmanned aerial vehicle. Measurement 138, 461–466. https://doi.org/10.1016/j.measurement.2019.02.023.

Peltier, W.R., 2002. On eustatic sea level history: last Glacial Maximum to Holocene. Quat. Sci. Rev. 21 (1–3), 377–396. https://doi.org/10.1016/s0277-3791(01)00084-1.

Peltier, W.R., 2004. Global glacial isostasy and the surface of the ice-age earth: the ICE-5G (VM2) model and GRACE. Annu. Rev. Earth Planet Sci. 32, 111–149. https://doi.org/10.1146/annurev.earth.32.082503.144359.

Peng, D., Hill, E.M., Meltzner, A.J., Switzer, A.D., 2019. Tide gauge records show that the 18.61-year nodal tidal cycle can change high water levels by up to 30 cm. Journal of Geophysical Research Oceans 124 (1), 736–749. https://doi.org/10.1029/2018jc014695.

Philibosian, B., Sieh, K., Avouac, J.-P., Natawidjaja, D.H., Chiang, H.-W., Wu, C.-C., Perfettini, H., Shen, C.-C., Daryono, M.R., Suwargadi, B.W., 2014. Rupture and variable coupling behavior of the Mentawai segment of the Sunda megathrust during the supercycle culmination of 1797 to 1833. J. Geophys. Res. Solid Earth 119 (9), 7258–7287. https://doi.org/10.1002/2014jb011200.

Piermattei, L., Carturan, L., de Blasi, F., Tarolli, P., Fontana, G.D., Vettore, A., Pfeifer, N., 2016. Suitability of ground-based SfM–MVS for monitoring glacial and periglacial processes. Earth Surf. Dyn. 4 (2), 425–443. https://doi.org/10.5194/esurf-4-425-2016.

Raoult, V., Reid-Anderson, S., Ferri, A., Williamson, J.E., 2017. How reliable is structure from motion (SfM) over time and between observers? A case study using coral reef bommies. Remote Sens. 9 (7), 740. https://doi.org/10.3390/rs9070740.

Riquelme, A., Tomás, R., Cano, M., Pastor, J.L., Jordá-Bordehore, L., 2021. Extraction of discontinuity sets of rocky slopes using iPhone-12 derived 3DPC and comparison to TLS and SfM datasets. IOP Conf. Ser. Earth Environ. Sci. 833 (1), 012056. https://doi.org/10.1088/1755-1315/833/1/012056.

Roering, J.J., Mackey, B.H., Marshall, J.A., Sweeney, K.E., Deligne, N.I., Booth, A.M., Handwerger, A.L., Cerovski, Darriau, C., 2013. 'You are HERE': connecting the dots with airborne lidar for geomorphic fieldwork. Geomorphology 200, 172–183. https://doi.org/10.1016/j.geomorph.2013.04.009.

Róg, M., Rzonca, A., 2021. The impact of photo overlap, the number of control points and the method of camera calibration on the accuracy of 3D model reconstruction. Geomatics and Environmental Engineering 15 (2), 67–87. https://doi.org/10.7494/geom.2021.15.2.67.

Rossi, P., Castagnetti, C., Capra, A., Brooks, A.J., Mancini, F., 2019. Detecting change in coral reef 3D structure using underwater photogrammetry: critical issues and performance metrics. Applied Geomatics 12 (S1), 3–17. https://doi.org/10.1007/s12518-019-00263-w.

Rovere, A., Stocchi, P., Vacchi, M., 2016. Eustatic and relative sea level changes. Curr. Clim. Change Rep. 2 (4), 221–231. https://doi.org/10.1007/s40641-016-0045-7.

Sanz-Ablanedo, E., Chandler, J.H., Rodríguez-Pérez, J.R., Ordóñez, C., 2018. Accuracy of Unmanned Aerial Vehicle (UAV) and SFM photogrammetry survey as a function of the number and location of ground control points used. Remote Sens. 10 (10), 1606. https://doi.org/10.3390/rs10101606.

Sarkawi, G.M., 2024. Insights from Coral Microatolls into Sea-Level Variability and Subduction Zone Behavior. Ph.D. thesis. Nanyang Technological University. doi:10.32657/10356/174449.

Scoffin, T.P., Stoddart, D.R., 1978. The nature and significance of microatolls. Phil. Trans. Roy. Soc. Lond. B Biol. Sci. 284, 99–122. https://doi.org/10.1098/rstb.1978.0055.

Scoffin, T.P., Le Tissier, M.D.A., 1998. Late Holocene sea level and reef-flat progradation, Phuket, South Thailand. Coral Reefs 17, 273–276. https://doi.org/10.1007/s003380050128.

Sedrati, M., Morales, J.A., El M'rini, A., Anthony, E.J., Bulot, G., Le Gall, R., Tadibaght, A., 2022. Using UAV and Structure-From-Motion photogrammetry for the detection of boulder movement by storms on a rocky shore platform in Laghdira, northwest Morocco. Remote Sens. 14 (16), 4102. https://doi.org/10.3390/rs14164102.

Siringan, F.P., Shen, C.-C., Lin, K., Abigania, M.I.T., Gong, S.-Y., 2016. Coral-based Holocene sea level of Paraoir, western Luzon, Philippines. J. Asian Earth Sci. 123, 61–66. https://doi.org/10.1016/j.jseaes.2016.03.022.

Slatton, K.C., Carter, W.E., Shrestha, R.L., Dietrich, W., 2007. Airborne Laser Swath Mapping: achieving the resolution and accuracy required for geosurficial research. Geophys. Res. Lett. 34 (23). https://doi.org/10.1029/2007gl031939.

Śledź, S., Ewertowski, M.W., Piekarczyk, J., 2021. Applications of unmanned aerial vehicle (UAV) surveys and Structure from Motion photogrammetry in glacial and periglacial geomorphology. Geomorphology 378, 107620. https://doi.org/10.1016/j.geomorph.2021.107620.

Smith, M.W., Carrivick, J.L., Quincey, D.J., 2015. Structure from motion photogrammetry in physical geography. Prog. Phys. Geogr. 40–2, 247–275. https://doi.org/10.1177/0309133315615805.

Snavely, N., Seitz, S.M., Szeliski, R., 2006. Photo tourism: exploring photo collections in 3D. In: Finnegan, J., Dorsey, J. (Eds.), SIGGRAPH '06: ACM SIGGRAPH, 30 July – 3 August 2006, pp. 835–846. Boston, Massachusetts. https://phototour.cs.washington.edu/Photo_Tourism.pdf.

Tamimi, R., 2022. Relative accuracy found within iPhone data collection. Int. Arch. Photogram. Rem. Sens. Spatial Inf. Sci. 303–308. https://doi.org/10.5194/isprs-archives-xliii-b2-2022-303-2022. XLIII-B2-2022.

Tan, F., Horton, B.P., Ke, L., Li, T., Quye-Sawyer, J., Lim, J.T.Y., Peng, D., Aw, Z., Wee, S. J., Yeo, J.Y., Haigh, I., Wang, X., Aung, L.T., Mitchell, A., Sarkawi, G., Li, X., Tan, N. S., Meltzner, A.J., 2024. Late Holocene relative sea-level records from coral microatolls in Singapore. Sci. Rep. 14, 13458. https://doi.org/10.1038/s41598-024-62937-9.

Tatsumi, S., Yamaguchi, K., Furuya, N., 2022. ForestScanner: a mobile application for measuring and mapping trees with LiDAR-equipped iPhone and iPad. Methods Ecol. Evol. 14 (7), 1603–1609. https://doi.org/10.1111/2041-210x.13900.

Tavani, S., Billi, A., Corradetti, A., Mercuri, M., Bosman, A., Cuffaro, M., Seers, T., Carmineti, E., 2022. Smartphone assisted fieldwork: towards the digital transition of geoscience fieldwork using LiDAR-equipped iPhones. Earth Sci. Rev. 227, 103969. https://doi.org/10.1016/j.earscirev.2022.103969.

Tondo, G.R., Riley, C., Morgenthal, G., 2023. Characterization of the iPhone LIDAR-Based Sensing System for vibration measurement and modal analysis. Sensors 23 (18), 7832. https://doi.org/10.3390/s23187832.

Vaccher, V., Hastewell, L., Devoto, S., Corradetti, A., Mantovani, M., Korbar, T., Furlani, S., 2023. The application of UAV-derived SfM-MVS photogrammetry for the investigation of storm wave boulder deposits on a small rocky island in the semi-enclosed Northern Adriatic Sea. Geomat. Nat. Hazards Risk 15 (1). https://doi.org/10.1080/19475705.2023.2295817.

Verhoeven, G., 2011. Taking computer vision aloft – archaeological three-dimensional reconstructions from aerial photographs with photoscan. Archaeol. Prospect. 18 (1), 67–73. https://doi.org/10.1002/arp.399.

Wan, J.X.W., Meltzner, A.J., Switzer, A.D., Lin, K., Wang, X., Bradley, S.L., Natawidjaja, D.H., Suwargadi, B.W., Horton, B.P., 2020. Relative sea-level stability and the radiocarbon marine reservoir correction at Natuna Island, Indonesia, since 6400 yr BP. Mar. Geol. 430, 106342. https://doi.org/10.1016/j.margeo.2020.106342.

Weil-Accardo, J., Feuillet, N., Jacques, E., Deschamps, P., Beauducel, F., Cabioch, G., Taponnier, P., Saurel, J.-M., Galetzka, J., 2016. Two hundred thirty years of relative sea level changes due to climate and megathrust tectonics recorded in coral microatolls of Martinique (French West Indies). J. Geophys. Res. Solid Earth 121 (4), 2873–2903. https://doi.org/10.1002/2015jb012406.

Westoby, M.J., Brasington, J., Glasser, N.F., Hambrey, M.J., Reynolds, J.M., 2012. 'Structure-from-Motion' photogrammetry: a low-cost, effective tool for geoscience applications. Geomorphology 179, 300–314. https://doi.org/10.1016/j.geomorph.2012.08.021.

Westoby, M.J., Lim, M., Hogg, M., Pound, M.J., Dunlop, L., Woodward, J., 2018. Cost-effective erosion monitoring of coastal cliffs. Coast. Eng. 138, 152–164. https://doi.org/10.1016/j.coastaleng.2018.04.008.

Whitehouse, P.L., 2018. Glacial isostatic adjustment modelling: historical perspectives, recent advances, and future directions. Earth Surf. Dyn. 6, 401–429. https://doi.org/10.5194/esurf-6-401-2018.

Woodroffe, C., McLean, R., 1990. Microatolls and recent sea level change on coral atolls. Nature 344 (6266), 531–534. https://doi.org/10.1038/344531a0.

Yu, K.-F., Zhao, J.-X., Done, T., Chen, T.-G., 2009. Microatoll record for large century-scale sea-level fluctuations in the mid-Holocene. Quat. Res. 71 (3), 354–360. https://doi.org/10.1016/j.yqres.2009.02.003.

Zachariasen, J., Sieh, K., Taylor, F.W., Edwards, R.L., Hantoro, W.S., 1999. Submergence and uplift associated with the giant 1833 Sumatran subduction earthquake: evidence from coral microatolls. J. Geophys. Res. Solid Earth 104 (B1), 895–919. https://doi.org/10.1029/1998JB900050.

Zachariasen, Sieh, K., Taylor, F.W., Hantoro, W.S., 2000. Modern vertical deformation above the sumatran subduction zone: paleogeodetic insights from coral microatolls. Bull. Seismol. Soc. Am. 90 (4), 897–913. https://doi.org/10.1785/0119980016.